Available online at www.sciencedirect.com
SCIENCE DIRECT
Geochimica et Cosmochimica Acta 70 (2006) 2885–2901
Geochimica
www.elsevier.com/locate/gca

Geochemical evolution of a shallow magma plumbing system during the last 500 years, Miyakejima volcano, Japan: Constraints from ^{238}U–^{230}Th–^{226}Ra systematics

Tetsuya Yokoyama *, Takeshi Kuritani, Katsura Kobayashi, Eizo Nakamura

The Pheasant Memorial Laboratory for Geochemistry and Cosmochemistry, Institute for Study of the Earth's Interior, Okayama University at Misasa, Tottori-ken 682-0193, Japan

Received 20 July 2005; accepted in revised form 24 February 2006

Abstract

In order to unravel magma processes and the geochemical evolution of shallow plumbing systems beneath active volcanoes, we investigated U-series disequilibria of rocks erupted over the past 500 years (1469–2000 AD) from Miyakejima volcano, Izu arc, Japan. Miyakejima volcanic rocks show ^{238}U–^{230}Th–^{226}Ra disequilibria with excess ^{238}U and ^{226}Ra, due to the addition of slab-derived fluids to the mantle wedge. Basaltic bombs of the 2000 AD eruption have the lowest ($^{230}Th/^{232}Th$) ratio compared to older Miyakejima eruptives, yielding the youngest ^{238}U–^{230}Th model age of 2 kyr. This reinforces our previous model that fluid release from the slab and subsequent magma generation in the mantle wedge beneath Miyakejima occur episodically on a several-kyr timescale. In the last 500 years, Miyakejima eruptives show: (1) a vertical trend in a ($^{230}Th/^{232}Th$)–($^{238}U/^{232}Th$) diagram and (2) a positive linear correlation in a $(^{226}Ra/^{230}Th)_0 - 1/^{230}Th$ diagram, which is also observed in lavas from some of the single eruptions (e.g., 1940, 1962, and 1983 AD). The variations cannot be produced by simple fractional crystallization in a magma chamber with radioactive decay of ^{230}Th and ^{226}Ra, but it is possibly produced by synchronous generation of melts in the mantle wedge with different upwelling rate or addition of multiple slab-derived fluids. A much more favorable scenario is that some basaltic magmas were intermittently supplied from deep in the mantle and injected into the crust, subsequently modifying the original magma composition and producing variations in ($^{230}Th/^{232}Th$) and $(^{226}Ra/^{230}Th)_0$ ratios via assimilation and fractional crystallization (AFC). The assimilant of the AFC process would be a volcanic edifice of previous Miyakejima magmatism. Due to the relatively short timescales involved, the interaction between the assimilant and recent Miyakejima magmatism has not been recorded by the Sr–Nd–Pb isotopic systems. In such cases, Th isotopes and ($^{226}Ra/^{230}Th$) ratio are excellent geochemical tracers of magmatic evolution.

1. Introduction

For investigation of various magma processes occurring in magma chambers beneath active volcanoes, it is important to know how each volcano has evolved and will evolve in the future. In addition to advancing knowledge about geochemical processes, such information is also potentially useful for predicting volcanic hazards. Constraints on timescales for individual processes, such as fractional crystallization, magma mixing and crustal assimilation, would give significant clues for quantitative evaluation of the evolution of a shallow magma plumbing system. Radioactive disequilibria of short-lived U-series nuclides in volcanic rocks are key geochemical tracers that enable direct dating of those magma processes, with timescales ranging from 10 to 350 kyr for ^{238}U–^{230}Th systematics, from 5 to 150 kyr for ^{235}U–^{231}Pa systematics, from 100 to 8000 yr for ^{230}Th–^{226}Ra systematics and from 1 to 30 yr

* Corresponding author. Present address: Department of Geology, University of Maryland, College Park, MD 20742, USA. Fax: +1 301 405 3597.

E-mail addresses: yoko@pheasant.misasa.okayama-u.ac.jp (T. Yokoyama), kuritani@misasa.okayama-u.ac.jp (T. Kuritani), katsura@pheasant.misasa.okayama-u.ac.jp (K. Kobayashi), eizonak@misasa.okayama-u.ac.jp (E. Nakamura).

0016-7037/$ - see front matter © 2006 Elsevier Inc. All rights reserved.
doi:10.1016/j.gca.2006.02.027

for ^{232}Th–^{228}Ra systematics (Ivanovich and Harmon, 1992; Bourdon et al., 2003). In particular, ^{230}Th–^{226}Ra disequilibrium is suitable for the study of shallow plumbing systems because repose time between eruptions is typically on a timescale from decades to several hundred years. Another advantage of the ^{230}Th–^{226}Ra systematics is that Ra is much more compatible in plagioclase and alkaline feldspar than Th, possibly resulting in ^{230}Th–^{226}Ra disequilibrium caused by fractional crystallization in a magma chamber with the involvement of those minerals.

Recent technical innovations to mass spectrometry techniques have enabled precise determination of ^{230}Th–^{226}Ra disequilibrium with an analytical error of around 1% (Goldstein and Stirling, 2003), and ^{230}Th–^{226}Ra systematics are now being quantitatively applied to the study of magma chamber processes (summarized in Condomines et al., 2003; Hawkesworth et al., 2004). One of the pioneering works is a case study of Mt. Etna, Italy, that was carried out by Condomines et al. (1995). That study revealed that magma differentiation from hawaiites to mugearites occurred on a short timescale (<200 yr) beneath Mt. Etna, and estimated a magma residence time in a steady-state deep reservoir (~20 km depth) to be <1500 yr. With the combination of ^{230}Th–^{226}Ra disequilibrium and model calculation, Vigier et al. (1999) determined crystallization ages for 1978 AD lavas of Ardoukoba volcano, Djibouti, to be 1880 and 870 yr for open- and closed system models, respectively. More recently, ^{230}Th–^{226}Ra disequilibrium was directly applied to plagioclase separates to precisely determine the timescales of crystal growth and residence time in a magma chamber (Cooper et al., 2001, 2003; Turner et al., 2003).

In this study, we have investigated ^{238}U–^{230}Th–^{226}Ra systematics of volcanic eruptives over the last ~500 years (1469–2000 AD) from the Miyakejima volcano, Izu arc, Japan, to reveal the timescale of magma processes and geochemical evolution in a shallow plumbing system beneath an active volcano. In the last 500 years, the Miyakejima volcano erupted frequently (at least 13 times), and each eruption age is verified by historic records. In addition, these eruptions have been well studied by geological, petrological and geochemical methods (e.g. Isshiki, 1960; Soya et al., 1984; Tsukui and Suzuki, 1998; Amma-Miyasaka and Nakagawa, 2002, 2003; Kuritani et al., 2003; Yokoyama et al., 2003). These well-characterized rocks provide us with an excellent opportunity to apply ^{238}U–^{230}Th–^{226}Ra systematics to Miyakejima volcano for better understanding of the evolution of a magma plumbing system as a function of time.

2. Geological setting

Miyakejima is an active volcano that belongs to the Izu arc, Japan (Lat. 34°05′ N, Long. 139°31′ E). The geology of the Miyakejima volcano is described elsewhere in detail (e.g. Isshiki, 1960), and it is outlined below. Based on previous tephrochronological studies (e.g. Tsukui and Suzuki, 1998) and the major element chemical compositions of eruptives, Yokoyama et al. (2003) divided the volcanic history of the Miyakejima volcano into four stages (Stage 1: earlier than 7000 BP, Stage 2: 7000–4000 BP, Stage 3: 2500 BP–1154 AD, Stage 4: 1469–1983 AD). This classification is followed in this paper as well, and we mainly focus on the volcanic activity of Stage 4 including the most recent eruption which occurred in 2000 AD. According to historical records, the Miyakejima volcano has erupted at least 13 times since 1469 AD, including the four most recent eruptions in 1940, 1962, 1983 and 2000 AD. Three hundred years of volcanic dormancy exists between Stages 3 and 4, and therefore it is possible that some dramatic changes occurred to the shallow magma plumbing system beneath Miyakejima before the onset of the Stage 4 activity. Repose times of eruptions during Stage 4 ranged from 17 to 69 years, and became shorter after 1940 AD. Except for the most recent eruption (2000 AD), volcanic ejecta (lavas and scoria) erupted from flank fissures, accompanied by summit eruptions in some cases (1469, 1535, 1811 and 1940 AD) (Tsukui and Suzuki, 1998). In contrast, the 2000 AD eruption started with the submarine eruption of June 27th, followed by the subsequent summit eruption of volcanic gases and tephra accompanied by the caldera collapse starting on July 8th (Nakada et al., 2001; Geshi et al., 2002a,b). The most active eruption took place on August 18th with the ejection of volcanic lapilli and bombs from the summit, and since then, SO_2 gas has been continuously discharged from the summit. However, no significant lava eruption occurred in the sequence of 2000 AD volcanic activity, which is remarkably different from the previous twelve eruptions in Stage 4.

3. Analytical methods

All the analyses were carried out at the Pheasant Memorial Laboratory, Okayama University (Nakamura et al., 2003). Trace elements and isotopes were handled under class 100 clean condition. We have already reported U-series isotope data of Miyakejima volcano for some Stage 4 samples as well as their major elements, trace elements and Sr–Nd–Pb isotopes in our previous studies (Kuritani et al., 2003; Yokoyama et al., 2003). In this study, we measured isotopes and abundances of U, Th, and Ra for 39 samples from 1940 to 1983 AD lavas and three bombs erupted on August 18th, 2000. In addition, major elements, trace elements and Sr–Nd–Pb isotopes were newly measured for some Stage 4 samples.

Analytical techniques for major elements, trace elements and Sr–Nd–Pb isotopes of whole rock samples were the same as described in Yokoyama et al. (2003). Lead isotope ratios were renormalized using the NBS981 value of Kuritani and Nakamura (2003) ($^{206}Pb/^{204}Pb = 16.9424$, $^{207}Pb/^{204}Pb = 15.5003$, $^{208}Pb/^{204}Pb = 36.7266$). Typical analytical reproducibility was 0.005%, 0.005% and 0.02% for Sr, Nd and Pb, respectively. U–Th–Ra isotope

measurement techniques were slightly modified from Yokoyama et al. (2003), and are briefly described here. Approximately 0.5 g of powdered sample were weighed and mixed with ^{229}Th, ^{233}U and ^{228}Ra enriched spikes simultaneously, then decomposed with HF–$HClO_4$ in a Teflon beaker following the method of Yokoyama et al. (1999a). The decomposed solution was dried and dissolved in 1.2 mL of 5 M HNO_3. It was centrifuged to separate white precipitates of Ti-oxides. Uranium, Th, and Ra were then separated by ion-exchange column chromatography as described in Yokoyama et al. (2003), with some modifications. The sample solution was loaded on the first column (0.5 mL of U/TEVA · spec, Eichrom Inc.), and the first 3 mL of the "Fraction I-1" of Yokoyama et al. (1999b), in which major elements were distributed, were collected for further separation of Ra. The rest of the procedure for U and Th separation was the same as Yokoyama et al. (2003). The major fraction containing Ra was dried and conditioned with 4.5 mL of 1 M HCl, and Ra was separated following the method described in Yokoyama and Nakamura (2004).

Isotope analyses of U, Th, and Ra were performed by using a thermal ionization mass spectrometer (TIMS, Finnigan MAT262 with RPQ_{plus}, "*INU*"), and details about the mass spectrometer and analytical procedures are presented in Yokoyama et al. (2001, 2003). For some samples, Ra was measured by a total evaporation TIMS (TE-TIMS) technique (Yokoyama and Nakamura, 2004), which enables more precise and accurate analysis compared to the conventional method that was used by Yokoyama et al. (2003). To confirm analytical reproducibility, five replicate measurements of a standard rock sample JB-2 (tholeiitic basalt of Izu-Oshima, Japan) obtained from the Geological Survey of Japan were carried out. Less than 0.5 g of powdered sample were used in each run. The standard has major element compositions similar to Miyakejima Stage 4 samples (Imai et al., 1995), and its Th and U concentrations are close to the minimum values of the Miyakejima Stage 4 samples. In the replicate analyses, we obtained $(^{230}Th/^{232}Th) = 1.250 \pm 0.013$, $Th = 0.2561 \pm 0.0022$ (μg/g), $(^{234}U/^{238}U) = 1.001 \pm 0.002$, $U = 0.1536 \pm 0.0013$ (μg/g) and $^{226}Ra = 81.1 \pm 0.5$ (fg/g), respectively (errors are 2σ). Radium was measured by TE-TIMS. Analytical reproducibilities for Th, U, and Ra concentrations were better than 1% as shown above, and this generally confirms isotopic equilibrium between samples and spikes during sample digestion and chemical separation. Total procedural blanks were <50 pg for Th and U, and ~0.03 fg for Ra, and they are negligible in this study.

Isotope ratios in parentheses represent activity ratios throughout this paper unless noted otherwise. Decay constants of U, Th, and Ra nuclides used for calculations in this study were as follows: $\lambda_{238U} = 1.55125 \times 10^{-10}$, $\lambda_{234U} = 2.8263 \times 10^{-6}$, $\lambda_{232Th} = 4.9475 \times 10^{-11}$, $\lambda_{230Th} = 9.158 \times 10^{-6}$, and $\lambda_{226Ra} = 4.332 \times 10^{-4}$ (Le Roux and Glendenin, 1963; Jaffey et al., 1971; Cheng et al., 2000).

4. Petrology and geochemistry

4.1. Petrology of Miyakejima eruptives

Volcanic rocks of Miyakejima consist of tholeiitic basalts, basaltic andesites and andesites ($SiO_2 = 48$–59%) with mineral assemblages of plagioclase ± olivine ± augite ± magnetite. Hypersthene is rare and hydrous minerals are absent in all samples. Most of the lavas erupted in Stage 4 are nearly aphyric containing <5% phenocrysts. Megacrysts of plagioclase (<30 mm) and olivine (<5 mm) occur rarely in some lavas (e.g., 1811, 1874, and 1940 AD), and are considered to be xenocrysts derived from basement plutonic rocks (Amma-Miyasaka and Nakagawa, 2002, 2003).

For 2000 AD eruption, there are two distinct types of eruptives (Geshi et al., 2002b). Basaltic andesite ($SiO_2 = 54\%$) erupted during June–July 2000 has mineralogical and geochemical characteristics that closely resemble the 1983 AD eruptives, indicating that these rocks were derived from the same magma chamber as for 1983 AD. The other type is basaltic bombs ($SiO_2 = 51.5\%$) erupted on August 18th, 2000, that contain 13–17 vol.% of plagioclase, 1 vol.% of olivine, and rare augite and magnetite. In this study, we used three basaltic bombs erupted on August 18th. In the following sections, "2000 AD samples" represent the basaltic bombs, and do not include basaltic andesites erupted before August 18th.

4.2. Major elements, trace elements and Sr–Nd–Pb isotopes

Major and trace element concentrations, and Sr–Nd–Pb isotopic compositions are listed in Table 1 for representative samples of Stage 4. Thorium and uranium concentrations determined by ID-TIMS are shown in Table 2. Figs. 1a–c depict Harker diagrams for TiO_2, MgO and K_2O plotted against SiO_2. Stage 4 samples, including 2000 AD eruptives, are enriched in SiO_2 compared to most of the previous stage samples, and they show a smooth composition trend regarding K_2O, which seems to be the effect of fractional crystallization. Some of the 1940 AD data that lie apart from the main trend are megacryst-bearing samples. We do not use these megacryst-bearing samples in the following discussion. A clear compositional gap between Stages 1–2 and Stages 3–4 data in the K_2O–SiO_2 diagram could indicate that Stages 3–4 magmas were not produced by fractional crystallization of Stages 1–2 magmas. In the MgO–SiO_2 diagram, however, the trend of the 1469–1874 AD samples deviates from the major trend of the 1940–2000 AD samples. Furthermore, the 1469–1874 AD data scatter in the TiO_2–SiO_2 diagram, not forming a clear trend. The 2000 AD samples also deviate from the trend of 1940–1983 AD in the TiO_2–SiO_2 diagram.

Similar to K_2O, trace element concentrations of the Stage 4 samples show monotonic increase against SiO_2 concentration with clear compositional gaps from Stages 1 to 2 data (e.g., Th: Fig. 1d). Typical island arc signatures; LILE enrichments, positive spikes of Sr and Pb and

Table 1
Major and trace elements, and Sr–Nd–Pb isotope data for representative samples of Miyakejima volcano in Stage 4

Sample:	1801	1802	1803	0106[a]	0107[b]	0108	0110[a]	0117	0127	0129	0134	0135	0136[b]	0137	0138[b]
Age:	2000 AD	2000 AD	2000 AD	1983 AD	1983 AD	1983 AD	1983 AD	1983 AD	1983 AD	1983 AD	1983 AD	1983 AD	1983 AD	1983 AD	1983 AD
(wt.%)															
SiO_2	51.46	51.36	51.37	53.33	53.49	53.19	53.23	52.86	52.84	52.82	52.83	53.14	54.82	54.23	55.24
TiO_2	1.16	1.13	1.16	1.40	1.40	1.37	1.35	1.37	1.36	1.36	1.36	1.35	1.32	1.31	1.30
Al_2O_3	17.18	17.48	17.19	14.56	14.69	14.86	14.96	15.05	15.08	15.02	15.03	15.01	15.08	14.84	14.99
Fe_2O_3[d]	12.80	12.54	12.80	14.71	14.62	14.48	14.15	14.30	14.30	14.32	14.28	14.09	13.61	13.50	13.31
MnO	0.21	0.20	0.20	0.24	0.24	0.24	0.24	0.24	0.24	0.24	0.24	0.24	0.24	0.23	0.23
MgO	4.23	4.16	4.19	4.14	4.10	4.08	3.95	4.01	4.00	4.00	4.01	3.93	3.76	3.71	3.68
CaO	10.62	10.70	10.62	8.86	8.90	9.05	8.96	9.13	9.14	9.11	9.11	8.97	8.62	8.50	8.43
Na_2O	2.40	2.38	2.39	2.81	2.79	2.79	2.81	2.76	2.77	2.77	2.74	2.82	2.94	2.88	3.01
K_2O	0.43	0.42	0.42	0.55	0.55	0.54	0.56	0.54	0.54	0.54	0.54	0.56	0.60	0.62	0.62
P_2O_5	0.12	0.12	0.12	0.16	0.16	0.15	0.15	0.15	0.15	0.15	0.15	0.15	0.16	0.16	0.16
L.O.I.	−0.75	−0.73	−0.68	−0.86	−0.76	−0.81	−0.80	−0.89	−0.79	−0.72	−0.76	−0.67	−0.85	−0.61	−0.85
Total	99.86	99.77	99.79	99.91	100.18	99.95	99.56	99.52	99.63	99.61	99.53	99.60	100.30	99.38	100.12
(μg/g)															
Cr_2O_3	76.9	72.7	77.5	35.7	38.1	36.8	34.1	36.1	33.5	33.6	32.4	33.7	36.1	30.7	32.2
NiO	15.2	15.7	15.1	10.6	8.70	9.62	7.80	7.24	8.74	8.50	7.67	7.97	9.82	8.20	9.19
(μg/g)															
Li	6.22	5.85	5.98	7.52	7.14	7.39	7.38	7.41	7.39	7.30	6.95	7.71	7.51	8.07	7.70
B	15.4	15.0	16.0	18.9	19.3	18.6	18.7	18.1	18.2	18.0	17.9	18.3	19.8	19.5	20.3
Rb	6.36	5.98	6.19	7.70	8.30	7.46	8.04	7.71	7.01	7.67	8.40	7.92	8.44	9.13	9.26
Sr	271	263	263	250	252	241	261	248	226	264	274	255	239	247	255
Y	28.3	26.8	28.1	34.3	38.1	32.9	35.3	35.1	31.5	34.3	38.1	34.4	35.9	37.0	39.1
Zr	51.7	50.1	50.5	64.5	65.0	62.4	64.9	62.5	61.5	58.8	60.9	59.9	69.3	68.6	72.3
Nb	0.435	0.406	0.412	0.536	0.573	0.508	0.534	0.512	0.503	0.512	0.509	0.518	0.594	0.541	0.570
Cs	0.449	0.435	0.430	0.578	0.584	0.545	0.569	0.529	0.481	0.556	0.597	0.544	0.604	0.598	0.647
Ba	166	161	164	194	214	191	205	194	178	196	220	210	215	229	235
La	2.94	2.80	2.85	3.76	3.74	3.37	3.58	3.46	3.24	3.62	3.71	3.81	3.83	3.95	4.01
Ce	8.49	8.27	8.42	10.6	11.0	10.2	10.7	9.97	9.00	10.5	11.2	10.4	11.3	11.4	12.0
Pr	1.52	1.40	1.44	1.81	1.91	1.60	1.89	1.63	1.58	1.77	1.93	1.93	1.89	1.83	2.01
Nd	8.25	7.92	8.07	9.88	10.5	9.51	10.1	9.53	8.68	9.88	11.1	10.1	10.4	10.8	11.1
Sm	2.73	2.68	2.71	3.26	3.57	3.09	3.29	3.29	2.96	3.31	3.64	3.37	3.49	3.54	3.79
Eu	1.02	0.999	1.02	1.20	1.29	1.15	1.24	1.15	1.10	1.18	1.34	1.13	1.26	1.20	1.29
Gd	3.61	3.41	3.45	4.29	4.70	4.19	4.43	4.26	3.99	4.35	4.45	4.14	4.61	4.54	4.81
Tb	0.689	0.660	0.670	0.851	0.872	0.793	0.824	0.756	0.721	0.801	0.884	0.798	0.863	0.855	0.908
Dy	4.56	4.33	4.36	5.53	5.79	5.19	5.49	5.38	4.91	5.32	5.97	5.51	5.75	5.65	6.03
Ho	1.01	0.945	0.984	1.21	1.29	1.18	1.18	1.18	1.08	1.17	1.31	1.20	1.26	1.25	1.33
Er	2.67	2.62	2.69	3.28	3.54	3.11	3.23	3.19	2.85	3.33	3.56	3.45	3.46	3.44	3.64
Tm	0.419	0.407	0.409	0.505	0.551	0.474	0.514	0.502	0.452	0.497	0.561	0.524	0.549	0.531	0.568
Yb	2.92	2.73	2.83	3.64	3.76	3.32	3.52	3.40	3.16	3.43	3.88	3.33	3.68	3.67	3.87
Lu	0.420	0.400	0.410	0.512	0.542	0.471	0.505	0.481	0.452	0.503	0.534	0.488	0.537	0.519	0.570
Hf	1.60	1.51	1.63	1.98	1.91	2.00	2.00	1.93	1.88	1.90	1.94	1.88	2.10	2.14	2.15
Ta	0.0386	0.0406	0.0403	0.0494	0.0486	0.0473	0.0483	0.0454	0.0466	0.0480	0.0450	0.0477	0.0484	0.0476	0.0475
Pb	2.76	2.65	2.68	3.45	3.61	3.49	3.58	3.47	2.90	3.50	3.83	3.50	3.53	5.00	3.76
$^{87}Sr/^{86}Sr$	0.70345	0.70346			0.70343		0.70345			0.70346			0.70345		0.70343
$^{143}Nd/^{144}Nd$	0.51309	0.51310			0.51308		0.51307			0.51310			0.51307		0.51307

$^{206}Pb/^{204}Pb$	18.310	18.306		18.278		18.293			18.283			18.306		18.312	
$^{207}Pb/^{204}Pb$	15.509	15.509		15.520		15.518			15.519			15.514		15.511	
$^{208}Pb/^{204}Pb$	38.114	38.115		38.119		38.127			38.119			38.125		38.125	
Sample:	0141[a]	0142[b]	0143	0146[b]	0149[b]	0150[a]	0155[b]	0317[b]	0318	2823	3019	0201	0231	0238	0259
Age:	1983 AD	1983 AD	1983 AD	1983 AD	1983 AD	1983 AD	1983 AD	1983 AD	1983 AD	1983 AD	1983 AD	1962 AD	1962 AD	1962 AD	1962 AD
(wt.%)															
SiO_2	54.39	54.52	53.38	53.39	53.66	53.60	54.21	53.89	53.28	53.92	52.81	55.40	55.26	53.66	54.54
TiO_2	1.31	1.33	1.34	1.36	1.35	1.34	1.35	1.37	1.35	1.34	1.37	1.32	1.33	1.37	1.34
Al_2O_3	14.88	15.14	14.92	15.16	15.18	14.96	15.15	14.95	14.87	15.02	15.07	14.55	14.54	14.47	14.46
Fe_2O_3[d]	13.48	13.76	13.93	14.24	14.00	13.90	13.97	14.20	14.15	13.86	14.31	13.45	13.52	14.28	13.77
MnO	0.23	0.24	0.24	0.24	0.23	0.23	0.24	0.24	0.24	0.23	0.24	0.24	0.24	0.24	0.24
MgO	3.70	3.82	3.88	4.00	3.89	3.86	3.87	3.95	3.96	3.85	4.00	3.56	3.59	4.05	3.77
CaO	8.53	8.77	8.81	9.09	8.96	8.83	8.90	8.86	8.89	8.82	9.11	7.95	7.97	8.58	8.21
Na_2O	2.93	2.93	2.83	2.81	2.82	2.85	2.87	2.87	2.82	2.86	2.78	3.11	3.04	2.84	2.99
K_2O	0.62	0.59	0.57	0.55	0.56	0.58	0.57	0.57	0.56	0.58	0.55	0.66	0.65	0.57	0.62
P_2O_5	0.16	0.16	0.15	0.15	0.15	0.15	0.15	0.15	0.15	0.16	0.15	0.17	0.17	0.16	0.17
L.O.I.	−0.69	−0.87	−0.55	−0.50	−0.66	−0.71	−0.81	−0.74	−0.82	−0.85	−0.80	−0.78	−0.60	−0.63	−0.83
Total	99.55	100.38	99.50	100.47	100.15	99.60	100.48	100.29	99.46	99.79	99.59	99.64	99.72	99.59	99.29
(μg/g)															
Cr_2O_3	28.1	35.7	30.8	38.2	38.1	33.2	37.8	41.6	33.0	32.1	33.2	19.2	16.1	23.5	22.5
NiO	6.89	9.76	6.45	9.43	11.0	7.01	9.64	11.4	6.09	6.30	8.32	3.80	3.17	7.88	6.81
(μg/g)															
Li	7.24	7.01	7.50	6.55	7.05	7.26	7.33	7.16	7.18	6.96	7.41	8.43	8.03	7.15	8.24
B	19.9	17.6	18.4	18.7	18.8	18.9	18.5	19.2	19.3	19.4	18.4	21.8	21.0	18.8	20.1
Rb	8.76	8.20	8.59	7.59	8.32	8.31	8.43	8.41	8.03	7.43	7.22	9.62	9.41	8.48	9.38
Sr	250	255	272	243	252	254	254	255	247	206	238	257	242	252	258
Y	33.5	38.1	35.4	35.2	35.8	35.0	37.8	38.1	35.7	31.2	34.4	38.2	39.5	36.4	40.6
Zr	69.5	68.0	62.0	66.5	64.6	65.0	66.7	66.5	66.5	70.7	60.5	73.9	75.6	66.0	69.0
Nb	0.557	0.571	0.552	0.529	0.564	0.561	0.587	0.568	0.524	0.548	0.526	0.629	0.631	0.554	0.600
Cs	0.598	0.532	0.624	0.551	0.593	0.598	0.600	0.594	0.562	0.523	0.515	0.675	0.680	0.625	0.665
Ba	217	216	219	200	210	204	216	210	204	193	196	249	243	216	245
La	3.94	3.74	3.89	3.46	3.79	3.60	3.78	3.75	3.56	3.28	3.52	4.15	4.25	3.70	4.28
Ce	11.5	11.3	11.3	10.4	10.8	10.4	11.1	10.8	10.5	9.26	9.86	12.6	12.1	11.2	12.2
Pr	1.88	1.86	1.91	1.69	1.87	1.77	1.85	1.86	1.78	1.56	1.69	2.08	2.18	1.88	2.10
Nd	10.7	10.6	10.6	9.67	10.3	10.3	10.5	10.4	10.0	8.90	10.0	11.7	11.3	10.8	11.6
Sm	3.51	3.40	3.51	3.32	3.40	3.51	3.42	3.48	3.44	3.02	3.43	3.67	3.69	3.32	3.82
Eu	1.25	1.31	1.34	1.17	1.25	1.18	1.24	1.25	1.24	1.08	1.14	1.39	1.37	1.24	1.39
Gd	4.65	4.53	4.50	4.26	4.38	4.42	4.62	4.61	4.40	3.93	4.38	5.06	4.84	4.65	4.96
Tb	0.862	0.861	0.879	0.801	0.839	0.829	0.856	0.870	0.829	0.723	0.781	0.952	0.937	0.851	0.949
Dy	5.65	5.71	5.58	5.32	5.51	5.41	5.59	5.76	5.55	4.72	5.11	6.23	5.98	5.51	6.25
Ho	1.29	1.28	1.23	1.18	1.23	1.20	1.26	1.23	1.24	1.10	1.16	1.38	1.36	1.28	1.37
Er	3.50	3.43	3.39	3.26	3.40	3.18	3.45	3.37	3.32	2.89	3.18	3.68	3.64	3.27	3.84
Tm	0.549	0.526	0.527	0.501	0.533	0.501	0.545	0.533	0.516	0.467	0.501	0.609	0.574	0.522	0.594
Yb	3.85	3.72	3.63	3.46	3.56	3.50	3.60	3.66	3.59	3.34	3.38	4.05	3.92	3.72	4.15
Lu	0.557	0.539	0.545	0.508	0.521	0.481	0.551	0.531	0.523	0.449	0.476	0.597	0.576	0.534	0.591
Hf	2.17	2.05	1.98	1.89	1.92	2.10	1.99	1.94	1.96	1.99	1.96	2.32	2.31	2.11	2.14
Ta	0.0521	0.0471	0.0486	0.0470	0.0494	0.0496	0.0519	0.0512	0.0460	0.0488	0.0475	0.0574	0.0564	0.0476	0.0558
Pb	3.56	3.53	3.75	3.30	3.57	3.46	3.40	3.47	3.56	3.15	5.76	4.01	4.22	3.86	3.96

(*continued on next page*)

Table 1 (*continued*)

Sample:	0141[a]	0142[b]	0143	0146[b]	0149[b]	0150[a]	0155[b]	0317[b]	0318	2823	3019	0201	0231	0238	0259
Age:	1983 AD	1983 AD	1983 AD	1983 AD	1983 AD	1983 AD	1983 AD	1983 AD	1983 AD	1983 AD	1983 AD	1962 AD	1962 AD	1962 AD	1962 AD
$^{87}Sr/^{86}Sr$		0.70338		0.70344	0.70346		0.70346	0.70349		0.70347	0.70348	0.70345		0.70346	
$^{143}Nd/^{144}Nd$		0.51308		0.51307	0.51307		0.51309	0.51307		0.51309	0.51308	0.51309		0.51309	
$^{206}Pb/^{204}Pb$	18.301	18.309		18.307	18.299		18.306	18.296		18.302	18.307	18.309		18.292	
$^{207}Pb/^{204}Pb$	15.506	15.513		15.510	15.516		15.514	15.519		15.512	15.511	15.513		15.517	
$^{208}Pb/^{204}Pb$	38.102	38.125		38.115	38.123		38.124	38.129		38.119	38.123	38.123		38.114	

Sample	2701	2704[a]	0212	0217[a]	0310	2702[a]	2709[a]	2902[a]	2903[a]	2901[a]	2817[a]	0301[a]	0101[a]	0103[c]	0104[a]	0115[a]
Age	1962 AD	1962 AD	1940 AD	1940 AD	1940 AD	1940 AD	1874 AD	1763 AD	1712 AD	1643 AD	1595 AD	1535 AD	1469 AD	1469 AD	1469 AD	9th C
(wt.%)																
SiO_2	54.11	54.95	54.47	56.17	54.45	56.54	53.96	53.83	51.95	51.98	51.90	52.29	54.34	52.97	54.63	51.46
TiO_2	1.37	1.34	1.35	1.27	1.29	1.23	1.26	1.34	1.31	1.35	1.17	1.18	1.17	1.28	1.19	1.26
Al_2O_3	14.55	14.56	14.53	14.71	14.74	14.76	15.56	14.59	14.72	14.64	15.29	15.29	14.92	14.92	14.88	15.62
Fe_2O_3[d]	14.19	13.77	13.89	12.60	13.43	12.46	13.19	14.00	14.44	14.83	13.59	13.51	12.82	13.74	12.89	14.18
MnO	0.24	0.24	0.24	0.24	0.24	0.23	0.23	0.24	0.24	0.24	0.23	0.23	0.22	0.23	0.22	0.23
MgO	4.00	3.74	3.84	3.35	3.88	3.38	3.88	3.96	4.76	4.81	5.14	4.91	4.32	4.46	4.17	4.38
CaO	8.55	8.19	8.29	7.70	8.42	7.76	8.99	8.41	9.59	9.66	9.96	9.79	8.93	9.00	8.76	9.97
Na_2O	2.87	3.02	2.93	3.16	2.93	3.18	2.82	2.88	2.55	2.57	2.42	2.49	2.75	2.67	2.82	2.51
K_2O	0.58	0.63	0.61	0.69	0.61	0.71	0.56	0.59	0.48	0.49	0.47	0.49	0.63	0.56	0.66	0.45
P_2O_5	0.16	0.17	0.17	0.18	0.16	0.18	0.16	0.15	0.14	0.14	0.13	0.13	0.15	0.14	0.16	0.13
L.O.I.	−0.84	−0.75	−0.73	−0.55	−0.74	−0.62	−0.64	−0.41	−0.60	−0.93	−0.64	−0.76	−0.70	−0.35	−0.52	−0.70
Total	99.79	99.88	99.60	99.52	99.41	99.81	99.99	99.59	99.57	99.79	99.67	99.55	99.57	99.64	99.86	99.50
(μg/g)																
Cr_2O_3	22.1	20.3	20.9	12.2	25.5	13.0	30.3	21.4	56.0	58.1	79.3	75.7	59.5	48.6	46.8	50.6
NiO	6.09	5.60	5.84	0.619	6.06	3.05	7.69	6.59	13.4	13.1	17.1	15.4	11.5	10.2	10.2	11.3
(μg/g)																
Li	7.80	8.22	7.45	8.34	6.96	8.86	6.44	7.49	6.59	6.49	5.68	5.47	7.76	7.04	7.39	6.43
B	19.4	20.4	20.5	21.4	20.2	21.5	17.9	19.1	16.9	16.0	15.9	14.9	20.3	17.9	20.9	15.4
Rb	8.22	9.52	9.19	10.1	8.49	10.3	8.03	8.52	7.13	6.96	6.39	6.96	9.21	8.12	9.49	6.21
Sr	249	259	261	244	229	243	259	262	258	243	233	245	225	236	243	245
Y	34.9	39.6	38.3	40.2	37.0	41.2	35.0	37.4	31.7	33.0	29.0	32.0	35.8	34.5	37.9	29.6
Zr	71.8	74.5	70.4	78.0	73.6	81.6	68.8	69.5	56.4	57.9	53.0	58.3	73.4	65.3	73.9	51.3
Nb	0.568	0.622	0.619	0.625	0.608	0.677	0.542	0.584	0.463	0.442	0.446	0.462	0.588	0.558	0.594	0.438
Cs	0.592	0.654	0.632	0.716	0.587	0.697	0.566	0.603	0.513	0.469	0.465	0.434	0.655	0.557	0.671	0.427
Ba	218	231	227	251	213	246	203	218	184	184	168	178	213	195	222	169
La	3.82	4.13	4.02	4.16	3.77	4.32	3.59	3.89	3.30	3.23	2.90	3.24	3.91	3.53	4.12	2.92
Ce	11.0	12.0	11.7	13.1	11.3	12.7	10.6	11.3	9.63	9.62	8.44	9.41	11.4	10.5	11.8	8.7
Pr	1.91	2.09	1.92	2.15	1.92	2.12	1.76	1.94	1.69	1.65	1.43	1.61	1.87	1.80	1.97	1.47
Nd	10.3	11.5	10.7	12.1	10.3	11.7	10.2	10.4	9.18	9.13	8.01	8.91	10.6	9.50	11.0	8.3
Sm	3.42	3.72	3.61	3.85	3.38	3.89	3.38	3.55	3.06	3.03	2.75	3.00	3.52	3.25	3.61	2.78
Eu	1.19	1.37	1.29	1.39	1.23	1.32	1.25	1.28	1.14	1.12	1.03	1.12	1.20	1.12	1.24	1.07
Gd	4.48	4.93	4.68	5.30	4.62	5.01	4.22	4.63	4.06	4.12	3.71	3.92	4.49	4.31	4.58	3.59
Tb	0.849	0.923	0.867	0.964	0.833	0.938	0.822	0.854	0.751	0.759	0.682	0.747	0.843	0.804	0.858	0.707
Dy	5.69	6.07	5.80	6.12	5.60	6.18	5.37	5.63	5.01	5.20	4.61	4.93	5.62	5.17	5.67	4.50
Ho	1.26	1.37	1.28	1.40	1.25	1.38	1.20	1.22	1.13	1.13	1.01	1.08	1.22	1.14	1.26	1.00
Er	3.41	3.71	3.58	3.80	3.46	3.74	3.22	3.44	3.10	3.13	2.73	2.93	3.34	3.09	3.44	2.73
Tm	0.510	0.592	0.547	0.595	0.526	0.591	0.502	0.518	0.481	0.480	0.424	0.452	0.521	0.494	0.528	0.420

Yb	3.68	4.03	3.65	4.17	3.62	4.05	3.49	3.56	3.26	3.33	2.95	3.17	3.53	3.34	3.79	2.98
Lu	0.528	0.588	0.526	0.601	0.544	0.594	0.518	0.534	0.467	0.479	0.426	0.459	0.526	0.474	0.526	0.422
Hf	2.09	2.16	2.21	2.37	2.19	2.41	2.02	2.08	1.78	1.78	1.64	1.75	2.22	2.02	2.31	1.61
Ta	0.0485	0.0541	0.0535	0.0543	0.0532	0.0595	0.0482	0.0509	0.0407	0.0396	0.0408	0.0403	0.0530	0.0500	0.0553	0.0396
Pb	4.46	3.96	3.85	4.16	3.58	4.00	3.39	3.45	2.75	3.09	2.72	3.20	3.48	3.10	3.61	2.66
$^{87}Sr/^{86}Sr$		0.70347	0.70345		0.70347	0.70347	0.70349				0.70346		0.70347	0.70344	0.70345	0.70345
$^{143}Nd/^{144}Nd$		0.51311	0.51309		0.51310	0.51310	0.51310						0.51310	0.51310	0.51310	0.51311
$^{206}Pb/^{204}Pb$		18.310	18.298		18.293	18.307	18.299	18.311	18.314	18.284	18.304	18.273	18.310	18.310	18.311	18.309
$^{207}Pb/^{204}Pb$		15.520	15.516		15.518	15.509	15.516	15.512	15.516	15.515	15.518	15.517	15.511	15.510	15.511	15.509
$^{208}Pb/^{204}Pb$		38.139	38.120		38.127	38.117	38.123	38.124	38.136	38.101	38.132	38.091	38.123	38.123	38.124	38.114

[a] Indicates that all data are taken from Table 1 of Yokoyama et al. (2003).
[b] Indicates that all data are taken from Table 1 of Kuritani et al. (2003).
[c] Indicates that major and trace element data are taken from Table 1 of Yokoyama et al. (2003).
[d] Total Fe as Fe_2O_3.

HFSE depletions; are observed in trace element patterns normalized to N-MORB (not shown). As shown in Table 2, Figs. 1e and f, Sr–Nd–Pb isotopic compositions of Miyakejima lavas are fairly constant irrespective of the SiO_2 variation from Stage 1 to the latest 2000 AD eruption ($^{87}Sr/^{86}Sr = 0.70338–0.70349$; $^{143}Nd/^{144}Nd = 0.51307–0.51311$; $^{206}Pb/^{204}Pb = 18.273–18.314$; $^{207}Pb/^{204}Pb = 15.506–15.520$; $^{208}Pb/^{204}Pb = 38.091–38.139$). The results give us the common perspective for the occurrence of Miyakejima magmas as discussed in Yokoyama et al. (2003): the extremely homogeneous isotopic signatures can be attributed mainly to the slab-derived fluid for Sr and Pb, but to the mantle wedge for Nd, resulting in very small isotopic changes for variable mantle-fluid mixtures. Based on Pb isotope systematics, the altered-MORB component is dominant in the fluid component beneath Miyakejima with very small involvement of a sediment component (~1%). These signatures suggest metasomatism of depleted mantle wedge by slab-derived fluids.

4.3. ^{238}U–^{230}Th disequilibrium of whole rock samples

U–Th–Ra isotope compositions for Stage 4 samples are listed in Table 2. All the Stage 4 samples possess a ($^{238}U/^{230}Th$) ratio greater than 1, which is generally attributed to the addition of slab-derived fluid to the mantle wedge. Fig. 2 is a U–Th equiline diagram plotting Stage 4 data and samples of earlier stages. The 2000 AD samples have ($^{230}Th/^{232}Th$) ratios ranging from 1.300 to 1.311, the range which is the lowest among all the Miyakejima data including previous stages. ($^{230}Th/^{232}Th$) ratios of all the Stage 4 samples before 2000 AD range from 1.356 to 1.404, and they have a linear trajectory nearly parallel to the equiline which is impossible to explain in terms of an isochron (Fig. 2). The variation of the ($^{230}Th/^{232}Th$) ratio for the Stage 4 samples (excluding 2000 AD) are 3.5%, and it is slightly larger than the analytical reproducibility of the standard, JB-2 (±1.0% in 2σ, see Section 3).

To confirm actual precision of ($^{230}Th/^{232}Th$) measurements, replicate analyses were made for some Stage 4 samples. As shown in Table 2, the differences of ($^{230}Th/^{232}Th$) ratio in the duplicate (or triplicate) measurements are always <0.5%. Indeed, JB-2 has Th concentration that is lower than any of the Stage 4 samples, and the reproducibility of ($^{230}Th/^{232}Th$) ratio for a basaltic standard (JB-3: Th = 1.271 μg/g) was 0.77% (Yokoyama et al., 2003). We estimate that the typical analytical error for ($^{230}Th/^{232}Th$) ratio is ±0.8% or less, and ±1.0% of the external precision is the worst scenario throughout this study. Therefore, the observed ($^{230}Th/^{232}Th$) variations are real in the Stage 4 samples. For Th and U concentrations, most of the replicate analyses resulted in <1% differences (Table 2), which are comparable to the reproducibility of the JB-2 measurements (0.85% for Th and 0.82% for U). We therefore estimate of analytical errors of 1% for Th and U concentrations in this study. One sample (#2704) showed 2% lower

Table 2
U-series data for whole rock samples of Miyakejima volcano in Stage 4

Sample	Age	Th (TIMS) (μg/g)	U (TIMS) (μg/g)	(^{230}Th/^{232}Th)	(^{238}U/^{232}Th)	(^{234}U/^{238}U)	^{226}Ra (fg/g)	(^{226}Ra/^{230}Th)	(^{226}Ra/^{230}Th)$_0$
1801	2000 AD	0.262	0.148	1.311 ± 0.006	1.712	0.999 ± 0.002	121.1 ± 0.6[c]	3.17	3.17
Replicate		0.262	0.148	1.319 ± 0.007	1.718	1.000 ± 0.002	120.8 ± 0.6[c]	3.15	3.15
1802	2000 AD	0.259	0.145	1.302 ± 0.006	1.695	1.000 ± 0.002	118.7 ± 0.4[c]	3.17	3.17
Replicate		0.260	0.145	1.313 ± 0.006	1.687	1.000 ± 0.002	118.6 ± 0.6[c]	3.12	3.12
1803	2000 AD	0.260	0.146	1.300 ± 0.005	1.711	1.001 ± 0.003	119.2 ± 0.5[c]	3.17	3.18
0106[b]	1983 AD	0.330	0.193	1.378 ± 0.006	1.780	1.001 ± 0.003	158.9 ± 0.8	3.14	3.16
0107	1983 AD	0.329	0.193	1.364 ± 0.006	1.776	1.002 ± 0.002	157.2 ± 0.6	3.15	3.17
0108	1983 AD	0.321	0.190	1.372 ± 0.008	1.799	0.997 ± 0.002	154.6 ± 0.7	3.16	3.17
0110[a]	1983 AD	0.335	0.197	1.376 ± 0.007	1.779	1.001 ± 0.002	153.7 ± 1.9	3.00	3.01
0117	1983 AD	0.319	0.188	1.366 ± 0.005	1.791	0.999 ± 0.002	153.4 ± 0.7	3.17	3.18
0127	1983 AD	0.313	0.187	1.382 ± 0.009	1.817	0.999 ± 0.002	150.4 ± 0.8[c]	3.13	3.15
0129	1983 AD	0.316	0.188	1.371 ± 0.005	1.805	0.998 ± 0.002	155.0 ± 0.9	3.22	3.23
0134	1983 AD	0.317	0.188	1.365 ± 0.005	1.797	0.998 ± 0.002	153.8 ± 0.6	3.20	3.22
0135	1983 AD	0.330	0.195	1.378 ± 0.005	1.794	1.000 ± 0.002	154.7 ± 1.4	3.06	3.08
0136	1983 AD	0.362	0.213	1.389 ± 0.005	1.788	1.001 ± 0.005	158.6 ± 0.8	2.83	2.85
0137	1983 AD	0.374	0.220	1.387 ± 0.008	1.786	0.999 ± 0.002	162.0 ± 0.8	2.81	2.82
Replicate		0.372		1.384 ± 0.006	1.798			2.83	2.85
0138	1983 AD	0.371	0.220	1.396 ± 0.005	1.794	0.998 ± 0.001	159.6 ± 0.7	2.77	2.78
0141[a]	1983 AD	0.370	0.218	1.404 ± 0.007	1.789	1.000 ± 0.002	164.4 ± 2.6	2.84	2.86
Replicate							160.7 ± 1.0[c]	2.78	2.80
0142	1983 AD	0.352	0.205	1.372 ± 0.005	1.764	1.001 ± 0.002	157.3 ± 1.1	2.93	2.95
0143	1983 AD	0.335	0.198	1.376 ± 0.004	1.795	1.000 ± 0.003	156.9 ± 0.8	3.06	3.07
0146	1983 AD	0.318	0.190	1.377 ± 0.005	1.808	1.001 ± 0.003	150.3 ± 0.8	3.08	3.10
Replicate		0.320	0.188	1.379 ± 0.005	1.783	1.001 ± 0.003	152.9 ± 0.8[c]	3.12	3.13
0149	1983 AD	0.332	0.196	1.371 ± 0.007	1.790	1.000 ± 0.002	154.7 ± 0.8	3.05	3.07
0150[a]	1983 AD	0.343	0.202	1.390 ± 0.008	1.788	1.001 ± 0.003	155.1 ± 1.6	2.93	2.94
0155	1983 AD	0.340	0.202	1.391 ± 0.004	1.800	0.999 ± 0.002	156.7 ± 0.7	2.98	3.00
0317	1983 AD	0.337	0.197	1.366 ± 0.007	1.775	1.000 ± 0.002	156.8 ± 0.7	3.06	3.08
0318	1983 AD	0.330	0.196	1.376 ± 0.006	1.801	1.001 ± 0.002	154.5 ± 0.8	3.05	3.07
2823	1983 AD	0.342	0.203	1.388 ± 0.005	1.804	1.001 ± 0.003	157.1 ± 0.7	2.97	2.99
3019[b]	1983 AD	0.317	0.188	1.379 ± 0.008	1.797	1.001 ± 0.002	153.6 ± 0.8	3.16	3.17
0201	1962 AD	0.395	0.234	1.379 ± 0.006	1.797	1.000 ± 0.002	174.2 ± 0.7	2.87	2.91
0202	1962 AD	0.392	0.233	1.391 ± 0.005	1.805	1.001 ± 0.003	170.9 ± 0.8[c]	2.82	2.85
0227	1962 AD	0.388	0.230	1.383 ± 0.006	1.794	0.998 ± 0.006	170.2 ± 0.7[c]	2.85	2.88
0230	1962 AD	0.377	0.222	1.373 ± 0.005	1.789	1.003 ± 0.004	165.7 ± 0.9[c]	2.88	2.91
0231	1962 AD	0.394	0.232	1.377 ± 0.006	1.790	1.000 ± 0.002	175.3 ± 1.0	2.91	2.94
0238	1962 AD	0.344	0.203	1.375 ± 0.007	1.796	0.999 ± 0.002	160.6 ± 1.1	3.06	3.09
0239	1962 AD	0.343	0.204	1.374 ± 0.005	1.805	0.999 ± 0.003	159.1 ± 0.7[c]	3.04	3.07
Replicate		0.344	0.206	1.369 ± 0.005	1.819	1.000 ± 0.003		3.03	3.07
0255	1962 AD	0.384	0.227	1.388 ± 0.004	1.795	1.003 ± 0.003	169.9 ± 3.0[c]	2.86	2.90
0257	1962 AD	0.363	0.212	1.369 ± 0.006	1.773	1.003 ± 0.004	162.7 ± 0.6[c]	2.94	2.97
0258	1962 AD	0.379	0.222	1.370 ± 0.005	1.782	1.000 ± 0.004	167.1 ± 0.6[c]	2.89	2.93
0259	1962 AD	0.372	0.220	1.383 ± 0.005	1.796	0.999 ± 0.002	169.4 ± 0.9	2.96	2.99
Replicate							171.3 ± 0.5[c]	2.99	3.03
2701	1962 AD	0.351	0.207	1.377 ± 0.006	1.792	1.000 ± 0.002	161.7 ± 1.1	3.01	3.04
2704[a]	1962 AD	0.384	0.219	1.374 ± 0.007	1.733	1.000 ± 0.002	167.0 ± 1.6	2.85	2.88
Replicate		0.376	0.221	1.376 ± 0.006	1.787	1.003 ± 0.003		2.90	2.93
Replicate		0.376	0.221	1.382 ± 0.005	1.783	1.002 ± 0.002		2.89	2.92
0208	1940 AD	0.369	0.219	1.390 ± 0.005	1.801	1.000 ± 0.003	165.4 ± 0.5[c]	2.90	2.95
0209	1940 AD	0.415	0.241	1.379 ± 0.007	1.761	0.998 ± 0.005	172.0 ± 0.6[c]	2.70	2.75
0211	1940 AD	0.385	0.228	1.390 ± 0.007	1.798	1.002 ± 0.002	170.4 ± 0.5[c]	2.86	2.91
0212	1940 AD	0.367	0.217	1.385 ± 0.005	1.790	0.998 ± 0.002	168.0 ± 0.7	2.97	3.02
0213	1940 AD	0.404	0.237	1.389 ± 0.005	1.778	1.001 ± 0.002	168.5 ± 3.2[c]	2.70	2.75
0217[b]	1940 AD	0.435	0.250	1.382 ± 0.006	1.745	1.000 ± 0.004	179.0 ± 1.0	2.67	2.72
0218	1940 AD	0.381	0.224	1.390 ± 0.007	1.786	1.003 ± 0.004	164.5 ± 0.5[c]	2.79	2.84
0220	1940 AD	0.421	0.247	1.398 ± 0.007	1.782	1.003 ± 0.002	172.4 ± 0.8[c]	2.64	2.68
0310	1940 AD	0.372	0.218	1.379 ± 0.005	1.776	0.999 ± 0.001	165.1 ± 0.7	2.89	2.95
0311	1940 AD	0.369	0.217	1.383 ± 0.006	1.779	1.003 ± 0.003	162.2 ± 1.0[c]	2.85	2.91
2702[a]	1940 AD	0.441	0.255	1.384 ± 0.007	1.757	1.002 ± 0.004	174.4 ± 1.2	2.57	2.61
2709[a]	1874 AD	0.344	0.201	1.373 ± 0.007	1.774	1.003 ± 0.003	149.1 ± 1.1	2.84	2.95
2902[b]	1763 AD	0.351	0.204	1.386 ± 0.008	1.766	1.000 ± 0.003	149.5 ± 0.6	2.76	2.96
2903[a]	1712 AD	0.280	0.163	1.363 ± 0.007	1.767	1.001 ± 0.003	125.3 ± 1.1	2.95	3.21
2901[a]	1643 AD	0.278	0.166	1.376 ± 0.007	1.811	1.000 ± 0.004	129.8 ± 1.6	3.05	3.39

Table 2 (*continued*)

Sample	Age	Th (TIMS) (μg/g)	U (TIMS) (μg/g)	(^{230}Th/^{232}Th)	(^{238}U/^{232}Th)	(^{234}U/^{238}U)	^{226}Ra (fg/g)	(^{226}Ra/^{230}Th)	(^{226}Ra/^{230}Th)$_0$
2817[a]	1595 AD	0.272	0.161	1.356 ± 0.009	1.794	1.003 ± 0.004	118.6 ± 0.9	2.90	3.27
0301[a]	1535 AD	0.302	0.175	1.366 ± 0.008	1.759	1.001 ± 0.002	120.1 ± 0.7	2.62	2.99
0101[b]	1469 AD	0.396	0.231	1.395 ± 0.009	1.767	0.997 ± 0.003	141.0 ± 1.1	2.30	2.64
0103[a]	1469 AD	0.348	0.199	1.367 ± 0.007	1.734	1.002 ± 0.002	131.3 ± 1.4	2.48	2.87
0104[b]	1469 AD	0.412	0.237	1.386 ± 0.004	1.748	1.003 ± 0.003	142.8 ± 0.7	2.25	2.57
0115[a]	9th C	0.273	0.156	1.334 ± 0.008	1.736	1.003 ± 0.004	101.9 ± 1.5	2.52	3.50

[a] Indicates that all data are taken from Table 1 of Yokoyama et al. (2003).
[b] Indicates that Th and U data are taken from Table 1 of Yokoyama et al. (2003).
[c] Indicates that Ra was measured by total evaporation TIMS technique.

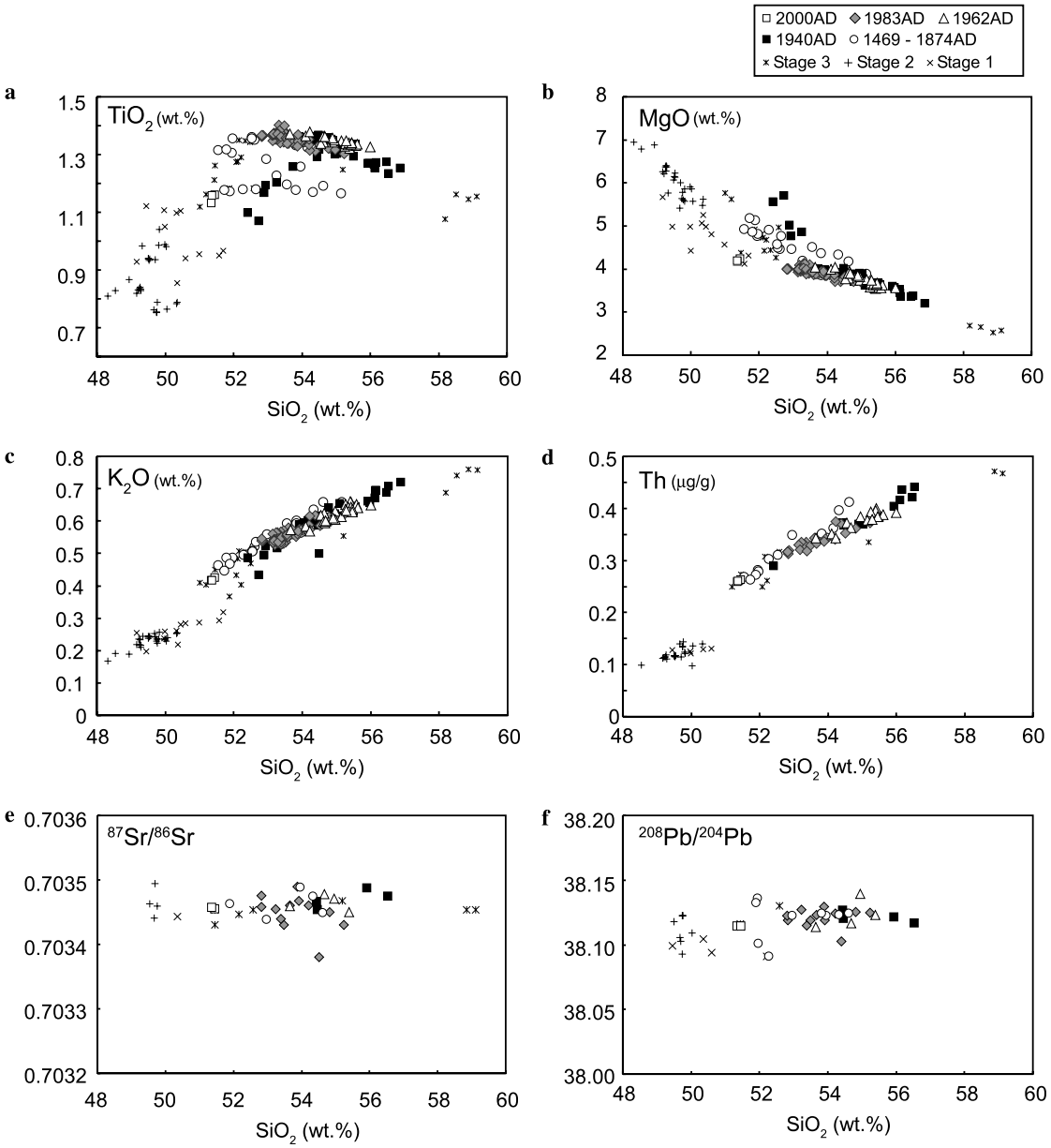

Fig. 1. SiO_2 variation diagrams of some major (TiO_2, MgO and K_2O) and trace (Th) elements, and $^{87}Sr/^{86}Sr$ and $^{208}Pb/^{204}Pb$ ratios for all stages of Miyakejima samples.

Th concentration in the replicate analysis, and further re-analysis also gave the 2% lower value. We attribute the mismatch to some error in the primary analysis (e.g., incomplete mixing between sample and spike), and we take the value of re-analysis for the sample #2704 in the following discussion.

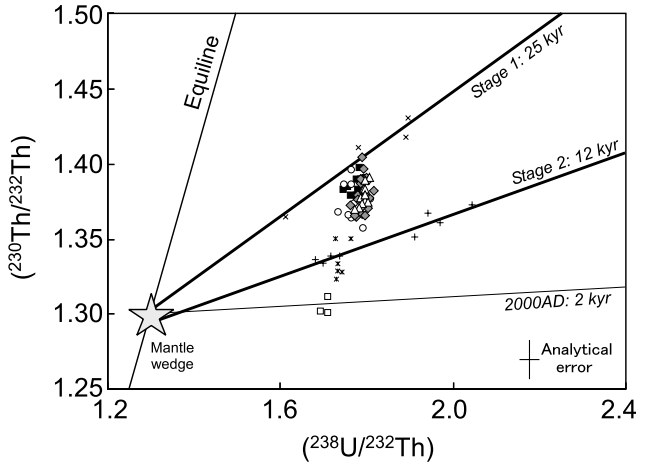

Fig. 2. U–Th equiline diagram for Miyakejima volcano. All the data are not corrected for time since eruption. A vertical trend of Stage 4 samples does not form any isochron. Star represents mantle wedge composition. Legends are the same as Fig. 1. Analytical error is calculated from the external precision of repeated analyses of a standard, JB-2 (1% for (^{230}Th/^{232}Th) and 1.4% for (^{238}U/^{232}Th)), which are the maximum estimates throughout this study.

4.4. ^{230}Th–^{226}Ra disequilibrium of whole rock samples

All of the Stage 4 samples have (^{230}Th/^{226}Ra) ratios greater than 1 (Table 2), considered to be the signature of the addition of slab-derived fluid to the mantle wedge. In Table 2, some of the replicate analyses for ^{226}Ra indicate 2% differences, which are beyond the reproducibility of JB-2 (0.61%). This is because Ra for JB-2 was measured by the TE-TIMS method. Replicate analyses that were both measured by the TE-TIMS are within the reproducibility of JB-2 (#1801, #1802). Therefore, we assume analytical errors of 2% for ^{226}Ra in this study, and discard previous ^{226}Ra values when re-analyzed by TE-TIMS. Propagation of analytical errors for Th and Ra analyses results in ~2.5% error in the (^{226}Ra/^{230}Th) ratio determined.

Similar to the (^{230}Th/^{232}Th) ratio, we observe a diversity of (^{226}Ra/^{230}Th) ratios in Stage 4 samples ranging from 2.25 to 3.22. This variation is markedly large compared to the analytical error for the (^{226}Ra/^{230}Th) ratio. The diversity remains even after correction of the (^{226}Ra/^{230}Th) ratio to the time of eruption ((^{226}Ra/^{230}Th)$_0$), although the range shifts somewhat (2.57–3.39). Fig. 3 shows the variation of the (^{226}Ra/^{230}Th)$_0$ ratio as a function of time ($e^{\lambda 226 \cdot t}$). The maximum (^{226}Ra/^{230}Th)$_0$ ratio in individual eruptions increases from 1469 AD towards 1643 AD, decreases towards 1874 AD, and then again increases until present. The diversity of (^{226}Ra/^{230}Th)$_0$ ratios exists in lavas from any single eruptions from 1940 to 1983 AD, and they cover whole the variation range present in Stage 4.

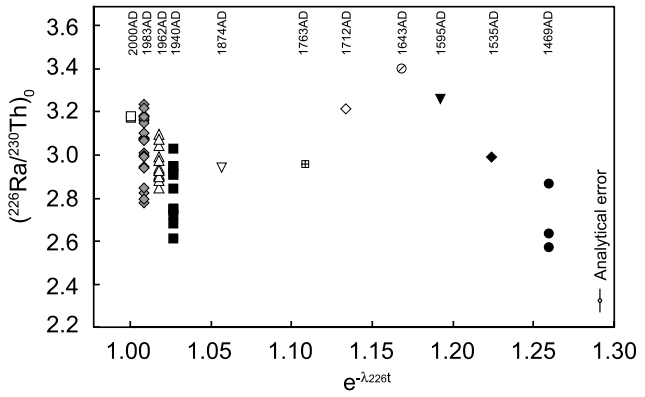

Fig. 3. Time change of (^{226}Ra/^{230}Th)$_0$ ratio (eruption time corrected value) for Miyakejima Stage 4 samples. Note that single eruptions from 1940 to 1983 AD have the variation of (^{226}Ra/^{230}Th)$_0$ ratio covering almost whole the range of Stage 4 eruptions.

5. Discussion

5.1. Origin of the 2000 AD magma

The 2000 AD samples have the lowest (^{230}Th/^{232}Th) ratios among all of the Miyakejima data including previous stages. Yokoyama et al. (2003) interpreted the two linear trends of Stage 1 and Stage 2 in Fig. 2 as isochrons that had different U–Th ages (25 and 12 kyr, respectively) but had a common initial Th isotopic ratio (star in Fig. 2) before the addition of the slab-derived fluid. The Stage 4 samples show a vertical array in the U–Th equiline diagram. If all of the Stage 4 samples originated from mantle wedge that had a common initial Th isotopic ratio as Stages 1 and 2, then we can calculate the "model ^{238}U–^{230}Th age" for these samples from the slope of a line tying each datum point and the star in Fig. 2. The model ages for the 2000 AD samples average 2 kyr, which is 10 kyr younger than that of Stage 2. It should be noted that, as previously discussed in Yokoyama et al. (2003), the determined ^{238}U–^{230}Th ages could be apparent ones which do not represent any absolute geological timescales, especially when slab-derived fluid contains some Th. Nevertheless, it is supposed that the relative differences in the ^{238}U–^{230}Th ages were created by different processes that led to the commencement of ^{238}U–^{230}Th disequilibrium, most likely the different timing of fluid release from the slab. Thus, the 10 kyr younger ^{238}U–^{230}Th age for the 2000 AD samples compared to Stage 2 supports the previous conclusion that fluid release from the slab and subsequent magma generation in the mantle wedge occur episodically on a several-kyr timescale beneath Miyakejima. In contrast, the model ages for the rest of Stage 4 samples range from 13.5 to 25 kyr, having a fairly longer timescale compared to the period of Stage 4 (500 yr). It is, thus, expected that some additional events (e.g., magma mixing) have disturbed the (^{230}Th/^{232}Th) ratios of these samples.

Fig. 4 shows (^{230}Th/^{232}Th) ratio of the Stage 4 samples plotted against 1/Th. The (^{230}Th/^{232}Th) ratios gradually decrease as Th concentrations decrease. This might be explained by a mixing between less-differentiated and differentiated magmas. If magma mixing is the cause of the variations of (^{230}Th/^{232}Th) ratios in the Stage 4 samples, one can expect from Fig. 2 that the 2000 AD samples are one of the mixing end-members. However, the trend for

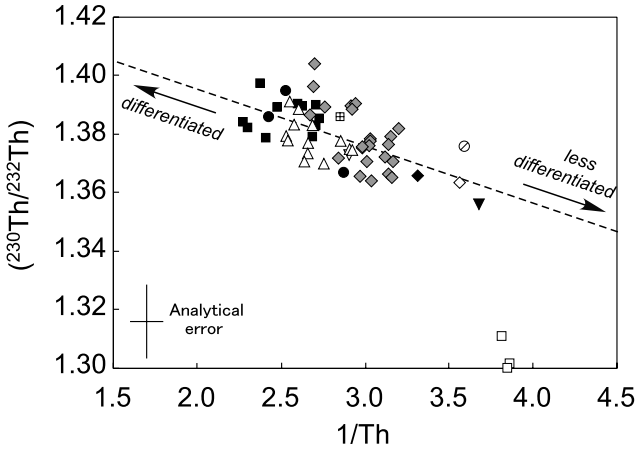

Fig. 4. (^{230}Th/^{232}Th) – 1/Th diagram for Stage 4 samples. Dashed line is a regression line except for 2000 AD data calculated by a least squares method. Symbols are the same as Fig. 3. Note that 2000 AD data deviate from the main trend. Estimation of analytical error is the same as Fig. 2.

Stage 4 samples, except for the 2000 AD in Fig. 4, demonstrates that the 2000 AD sample is not an acceptable end-member.

Fig. 5 is the relationship between (^{226}Ra/^{230}Th)$_0$ ratios and 1/^{230}Th for the Stage 4 samples. Assuming 1/^{230}Th as an index of magma differentiation, it is obvious that less differentiated samples have higher (^{226}Ra/^{230}Th)$_0$ ratios compared to the differentiated ones. A near-linear correlation observed for the Stage 4 samples suggests binary mixing between less differentiated magma with higher ^{230}Th–^{226}Ra and differentiated magma having lower ^{230}Th–^{226}Ra disequilibrium. Similar to the (^{230}Th/^{232}Th) – 1/Th diagram, the 2000 AD data slightly deviate from the linear trend, also indicating that the 2000 AD sample is not the mixing end component.

In addition to U–Th–Ra characteristics, some major element compositions of 2000 AD lie off the trend of Stage 4 (e.g., TiO_2, MgO; Fig. 1). Consequently, the 2000 AD magma is not the end-component of the main trend of the Stage

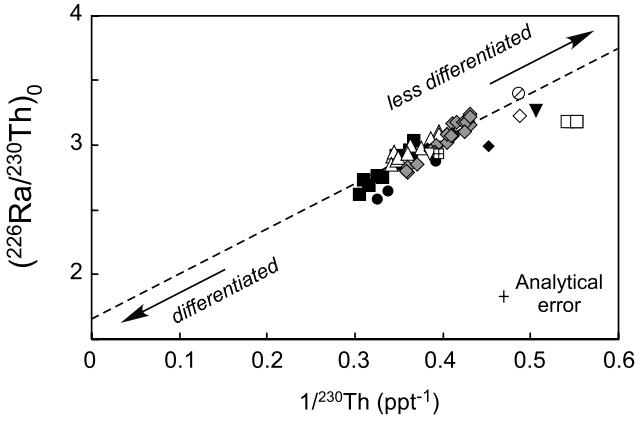

Fig. 5. (^{226}Ra/^{230}Th)$_0$ – 1/^{230}Th diagram for Stage 4 samples. Dashed line is a regression line except for 2000 AD data calculated by a least squares method. Symbols are the same as Fig. 3. Analytical error of (^{226}Ra/^{230}Th) is estimated to be 2.5%.

4 samples, but it might be fractionated from the end-member magma, or it was a new magma batch that had a completely different chemical composition.

5.2. Fractional crystallization with ^{226}Ra decay

It is noteworthy that the chemical diversity of the Miyakejima volcano with respect to (^{226}Ra/^{230}Th) ratio is also observed in individual lavas from some single eruptions (e.g., 1940, 1962, and 1983 AD). It has been reported that the (^{226}Ra/^{230}Th) ratio can vary during a single eruption in some volcanoes. Vigier et al. (1999) found that the (^{226}Ra/^{230}Th) ratio in basaltic lavas of Ardoukoba volcano (Asal rift, Djibouti) erupted in 1978 AD decreases with increasing Th concentration. They concluded that the variation arose from successive magma reinjections beneath the volcano, resulting in a chemically zoned magma chamber that was composed of previously injected, more crystallized old magma and recently injected, least crystallized young magma. Recently, Blake and Rogers (2005) demonstrated a mathematical model for the evolution of the (^{226}Ra/^{230}Th) ratio during simultaneous fractional crystallization and ageing of magma. They showed that the Ra–Th trend of Ardoukoba volcano could be created by 1570–2500 yr of the differentiation time (depending on the rate of fractionation). They also applied the model to Miyakejima data obtained from Yokoyama et al. (2003), and concluded that the Miyakejima data were best fitted with the differentiation time of 500–1600 yr.

The model of Blake and Rogers (2005) (linear model: Eqs. (1)–(3) of their paper) was applied to our Stage 4 data obtained here. Unlike Blake and Rogers (2005), the amount of ^{230}Th produced by the decay of ^{234}U was taken into account. The least differentiated sample (#2817) in Stage 4 was used as a starting material, and bulk partition coefficients used are described in Appendix A. As shown in Fig. 6a, a fractionation rate of 6×10^{-4} yr^{-1} gives the best fit evolution curve in the (^{226}Ra/^{230}Th)$_0$ – 1/^{230}Th diagram (bold curve). This requires approximately 800 yr of the differentiation time, which is within the range of the result of Blake and Rogers (2005). However, when the model is applied to the evolution of the (^{238}U/^{230}Th) ratio, all of the data fall far off the ^{238}U–^{230}Th–^{226}Ra "concordia" curve (Fig. 6b, bold curve). This clearly indicates that the most differentiated Stage 4 sample cannot be created by fractionation and ageing of magma which initially had the same (^{238}U/^{230}Th) and (^{226}Ra/^{230}Th) ratios as the sample #2817. Alternatively, a long differentiation time (80 kyr) coupled with a very slow fractionation rate (1×10^{-5} yr^{-1}) can yield a highly differentiated end member magma (Fig. 6, thin curves). It is possible to create the linear correlation observed in Fig. 6b when this differentiated magma is mixed with the less differentiated initial magma (dashed line). However, as can be seen in Fig. 5, extrapolation of the mixing array towards 1/^{230}Th = 0 shows that, under any condition, the more differentiated end-member must have a ^{226}Ra excess. Consequently, the

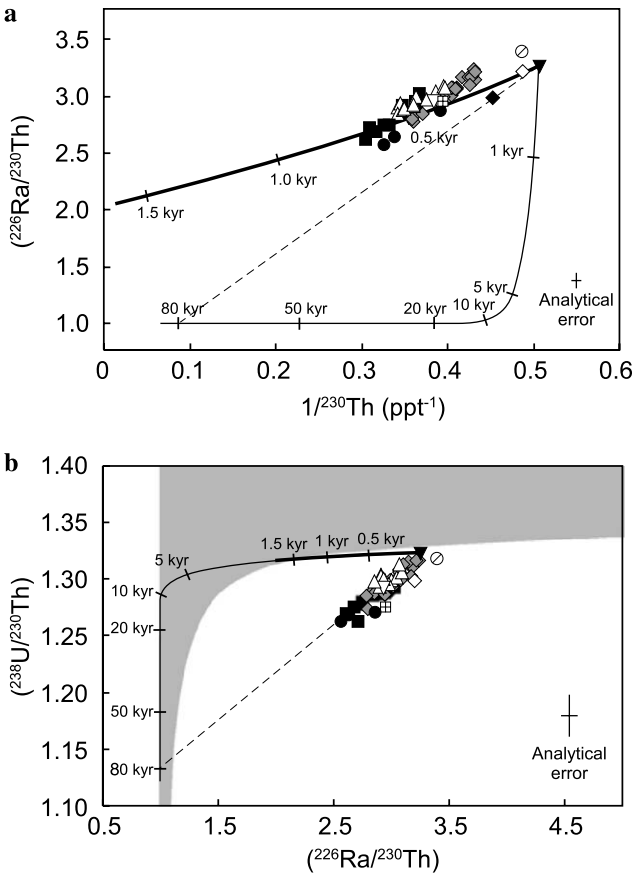

Fig. 6. (a) (^{226}Ra/^{230}Th) – 1/^{230}Th diagram and (b) (^{238}U/^{230}Th) – (^{226}Ra/^{230}Th) diagram for Stage 4 samples excluding 2000 AD. Eruption time correction is done for (^{226}Ra/^{230}Th) ratio of Miyakejima data. Bold and thin curves represent ^{238}U–^{230}Th–^{226}Ra "concordia" curves evolved in a closed system magma chamber by fractional crystallization and radioactive decay of ^{230}Th and ^{226}Ra with fractionation rates of 6×10^{-4} and 1×10^{-5} yr^{-1}, respectively. The least differentiated sample of Stage 4 (#2817) was used as a starting material. Dashed lines show mixing line between the starting material and evolved magma with differentiation time of 80 kyr. The gray zone in (b) is the result of melt or fluid replenishment model after Asmerom et al. (2005). Degree of fractionation per batch and interval of reinjections were varied from 0.001 to 0.8 and from 50 to 500 yr, respectively. Initial chemical composition of melt were varied from 1.35 to 2.0 for (^{238}U/^{230}Th) and from 4 to 10 for (^{226}Ra/^{230}Th), and that for fluid were varied from 2 to 10 for (^{238}U/^{230}Th) and from 50 to 100 for (^{226}Ra/^{230}Th). Concentration of Ra in fluid was set as to be 1% of magma. Analytical error is the maximum estimation. Symbols are the same as Fig. 3.

simple magma mixing model between a newly injected magma and an old magma stored in a magma chamber is not consistent with observations.

Discordant U-series ages are also observed for volcanic eruptives obtained from Taal volcano, Luzon Arc, Philippine. Asmerom et al. (2005) showed that the ^{235}U–^{231}Pa data of Taal volcano gave a differentiation time of ~30 kyr using a closed system magma fractionation model, although the ^{230}Th–^{226}Ra system gave a considerably younger timescale of a few kyr. They successfully explained the decoupling of ^{235}U–^{231}Pa and ^{230}Th–^{226}Ra ages by applying a magma (or fluid) replenishment model originally proposed by Hughes and Hawkesworth (1999). However, when their model is applied to the Miyakejima data, any combination of plausible parameters regarding replenishment frequency, degree of fractionation, and initial U–Th–Ra concentrations for magma (or fluid) does not give a concordant curve that can account for the Stage 4 data (gray area of Fig. 6b). Therefore, we conclude that fractional crystallization with ^{226}Ra decay is not suitable to explain the U-series systematics of Miyakejima Stage 4 data, even if the effects of magma or fluid replenishment are taken into account.

5.3. Chemical heterogeneity in primary melts

Here, we consider the generation of two or more chemically different but synchronous mantle-sourced melts that have (^{230}Th/^{232}Th) and (^{226}Ra/^{230}Th) ratios ranging from 1.30 to 1.40 and from 2.25 to 3.22 (the values at the time of eruption), respectively. This could occur when multiple slab-derived fluids, which individually had different (^{230}Th/^{232}Th) and (^{226}Ra/^{230}Th) ratios, contributed to a chemically homogeneous mantle source. In this case, it is assumed that the multiple fluids were released from the slab at short intervals of <1 kyr to create the variable (^{226}Ra/^{230}Th) ratios observed, rather than releasing every few thousand years, as discussed in Yokoyama et al. (2003). In addition, it is assumed that the multiple fluids had originally different (^{230}Th/^{232}Th) ratios at the time of fluid release, because the short interval of the fluid release is not long enough to create the observed variation in (^{230}Th/^{232}Th) ratio by ^{230}Th decay. The variable (^{230}Th/^{232}Th) ratio in the fluids is presumed to originate from chemical heterogeneity in the subducted altered oceanic crust. However, the other geochemical tracers for slab-derived fluid, such as Sr and Pb isotope ratios, are rather constant for Stage 4 samples (Figs. 1e and f), and do not systematically vary with the change of (^{230}Th/^{232}Th) and (^{226}Ra/^{230}Th) ratios. This reduces the likelihood of multiple slab-derived fluids model unless heterogeneity of Sr and Pb isotopes in the fluids are too small to be detected by our present analytical capability.

Alternatively, as demonstrated by George et al. (2003), vertical array in the U–Th equiline diagram for subduction zone samples could be produced by dynamic partial melting of U enriched sources with different velocities for mantle upwelling through the melting region. Their calculation showed that ^{226}Ra–^{230}Th fractionation was largely controlled by the residual porosity rather than the mantle upwelling rate. Therefore, the variation of (^{230}Th/^{232}Th) and (^{226}Ra/^{230}Th) ratios for the Stage 4 samples could be explained by multiple mantle melting with different upwelling rates and residual porosities. Otherwise the (^{226}Ra/^{230}Th) variations must simply represent different timing of melt segregation when there is no distinct difference in the residual porosity. To account for the change of (^{226}Ra/^{230}Th)$_0$ ratios with time, as well as (^{230}Th/^{232}Th) ratios during the 500 yr of Stage 4 (Figs.

2 and 5), it is presumed that more than two magma batches produced by different upwelling speeds (and residual porosities) intruded beneath Miyakejima and formed a chemically heterogeneous magma chamber by mixing. It remains unclear whether it is geophysically possible to produce two end-component magmas for the 1940–1983 AD eruptions in the mantle wedge synchronously but differently in terms of space, upwelling speed and residual porosity. Nevertheless, we cannot completely reject the multiple melt generation models, whether induced by multiple fluid additions or different mantle upwelling speeds.

5.4. Crustal assimilation and fractional crystallization

5.4.1. Basic model

Finally, as the most plausible scenario, we propose that crustal assimilation accompanied with fractional crystallization (AFC) played an important role in producing the trends of Stage 4 samples observed in Figs. 4 and 5. For simplification, we first apply the most basic AFC model (DePaolo, 1981) to Stage 4 samples:

$$C_m = C_m^0 \cdot F^{-z} + \left(\frac{r}{r-1}\right) \cdot \frac{C_a}{z} \cdot (1 - F^{-z}), \quad (1)$$

where F is the fraction of melt remaining, r is the ratio of assimilation rate and crystallization rate, $z = (r + D - 1)/(r - 1)$, D is the bulk partition coefficient of an element between crystal and melt, and C_m and C_a are concentrations in melt and assimilant, respectively. In this model, all U-series nuclides including ^{226}Ra are treated as stable isotopes, assuming the case when the duration of AFC is very short compared to the half-life of ^{226}Ra (1600 yr).

It should be noted that a linear trend in Fig. 5 is obtained using eruption time corrected (^{226}Ra/^{230}Th) data. If all the Stage 4 samples are produced by a single AFC process in a single magma chamber, then recent eruptives (e.g., 1983 AD) must have, owing to ^{226}Ra decay, (^{226}Ra/^{230}Th)$_0$ ratios lower than that of the earlier Stage 4 eruptions. This is clearly not the case. Hence, we expect that two or more different magma batches tapped into the crust and created individual magma chambers, having individual AFC trends for Stage 4 eruptions. However, these injected magmas would essentially have similar compositions including (^{226}Ra/^{230}Th) ratio at the time of injection, so that they ultimately produced a uniform AFC trend for entire Stage 4 samples except for 2000 AD as shown in Figs. 4 and 5. We assume that all the AFC parameters (e.g., r, C_m^0 and C_a) but F value are common for all the Stage 4 samples (excluding 2000 AD), and the least differentiated sample of Stage 4, #2817 (1595 AD), is chosen as the starting compositions in the AFC calculation. Bulk partition coefficients used in the calculation are described in Appendix A.

The ^{238}U–^{230}Th–^{226}Ra systematics observed implies that the assimilant should be a highly differentiated chemical component sufficient to increase Th concentrations in the magma. Isshiki (1960) showed that the basement rock of Miyakejima comprised some thermally altered rocks which resemble Miocene Yugashima rocks observed in the Izu peninsula. These rocks are expected to have Sr–Nd–Pb isotope ratios different from those of Miyakejima volcanic rocks, although no significant variations in Sr, Nd and Pb isotope ratios are found for any of the Stage 4 rocks. Thus, they are not a likely option for the assimilated crustal material. Fujii et al. (1984) found some xenoliths which have dacitic composition ($SiO_2 = 68\%$) in the 1983 AD lava flows. They also showed that the major element composition of the xenoliths lay on the extrapolation of a differentiation trend of Miyakejima magma, suggesting that these felsic xenoliths were genetically related to previous Miyakejima magmatism. When constant Sr–Nd–Pb isotopic compositions of the Stage 4 samples are taken into account, it is supposed that the assimilant has a genetic relation with prior Miyakejima magmas. We thus propose that the likely assimilated crustal material is volcanic edifice beneath Miyakejima that has solidified after the eruption of felsic rocks.

From Fig. 4, it can be shown that the (^{230}Th/^{232}Th) ratio of the assimilant must be high (>1.4) and therefore, assuming that it was also derived from a source with (^{230}Th/^{232}Th) = 1.3, the assimilated crustal material is sufficiently old for ^{230}Th–^{226}Ra equilibrium. By extrapolating the differentiation trend of SiO_2-Th diagram for all stages of Miyakejima rocks (Fig. 1d), the Th concentration of the assimilated crustal material is estimated to be 1 μg/g when SiO_2 reaches 70% by differentiation. In the basic model, we consider bulk assimilation of the crustal material in the AFC calculation, in which the chemical composition of the assimilant matches the bulk composition of the assimilated crustal material. We thus fixed (^{226}Ra/^{230}Th) = 1 and Th = 1 μg/g for the assimilant.

Two AFC parameters, r and (^{230}Th/^{232}Th)$_a$, are still unknown. To determine these parameters, we examined least squares calculations of AFC trends as a function of F in Th-(^{230}Th/^{232}Th)-^{226}Ra$_0$ space. Optimized AFC parameters that give the minimum residual are calculated to be (^{230}Th/^{232}Th)$_a$ = 1.57 and r = 0.23. By means of these parameters, the AFC trends are plotted on the (^{226}Ra/^{230}Th) − 1/^{230}Th and the (^{230}Th/^{232}Th) − 1/Th diagrams (Fig. 7). Broken lines in Fig. 7 represent bulk mixing between the starting material of AFC and the assimilant. The best fit AFC trends in this figure deviate from the bulk mixing lines and the (^{226}Ra/^{230}Th) ratio is still higher than 1 when 1/^{230}Th is close to 0. The AFC trend of $r = 0$, which represents the line of no assimilation, is almost flat in Fig. 7a and deviates from the best fit AFC trend. This means that the decrease in (^{226}Ra/^{230}Th) ratio for Stage 4 samples was caused mainly by assimilation with little Ra–Th fractionation by crystallization. Fractional crystallization, on the other hand, changed 1/^{230}Th significantly. The variation of (^{226}Ra/^{230}Th)$_0$ ratio is attributed to different F values for each sample. Therefore, (^{226}Ra/^{230}Th)$_0$ variations observed in single eruptions (e.g., 1940, 1962,

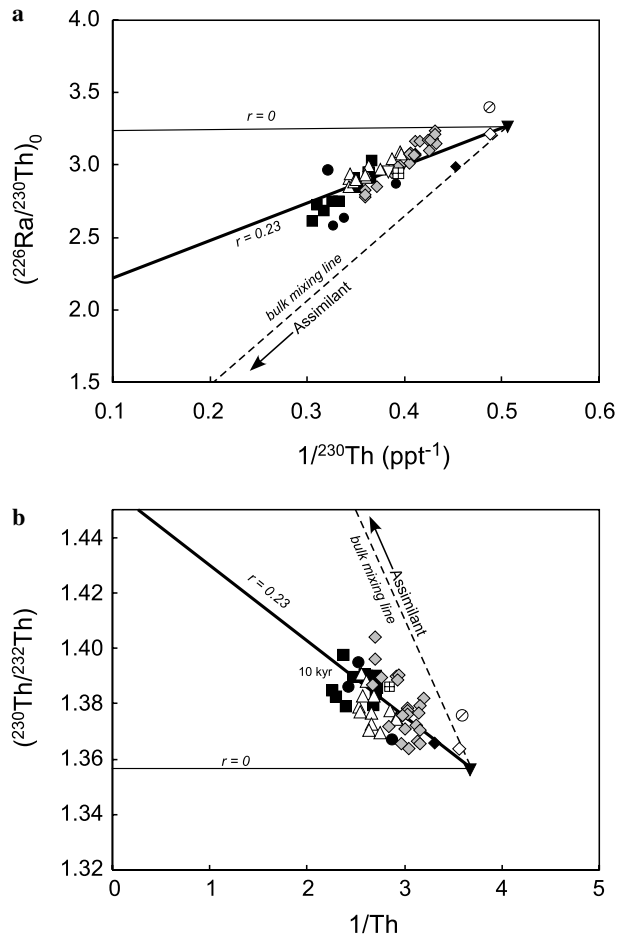

Fig. 7. AFC trajectories in (a) ($^{226}Ra/^{230}Th$) – $1/^{230}Th$ diagram and (b) ($^{230}Th/^{232}Th$) – 1/Th diagram applying the basic model of DePaolo (1981). Symbols are the same as Fig. 3. Thin and dashed lines represent fractional crystallization without assimilation ($r = 0$) and bulk mixing between injected magma and assimilant, respectively.

and 1983 AD) were created by spatial variation of F value in a magma chamber, which presumably corresponds to spatial difference of some physical parameters in the magma chamber (e.g., temperature, distance from the wall rock). However actual compositional heterogeneity in a magma chamber would not be so simple and can be easily perturbed by physical processes, such as thermal convection of the magma.

Compared to Fig. 7a, the Miyakejima data largely scatter in the ($^{230}Th/^{232}Th$) – 1/Th diagram (Fig. 7b). This is the result of the relatively large analytical error of the ($^{230}Th/^{232}Th$) ratio compared to the actual variation of ($^{230}Th/^{232}Th$) ratios for Stage 4 samples, indicating better resolution of the ($^{226}Ra/^{230}Th$) ratio as for a tracer to understand geochemical evolution of a magma plumbing system on a very short timescale like <500 years.

5.4.2. Advanced AFC model 1: partial melting of crust

Although we assumed bulk assimilation of crustal material in the basic AFC model above, it is also possible that the crustal melt, namely the assimilant, is not produced by bulk melting but partial melting of the surrounding crust leaving a residual solid phase in the wall of magma chamber. This can occur when the heat transfer is not sufficient to entirely melt the crustal material. If this is the case, Th concentrations in the crustal melts can be much larger than that of the crust because Th is extremely incompatible. Furthermore, the ($^{226}Ra/^{230}Th$) ratio of the melt could be fractionated and no longer be unity, even though the crust is old. To determine the Th concentration and ($^{226}Ra/^{230}Th$) ratio of the crustal melt, the degree of melting of the crust and solid/melt partition coefficients of the assimilated material are needed. This information is not easily to be fixed.

From Figs. 1c and d, it is clear that K_2O and Th are very well correlated for the whole Stage 4 samples, and a linear trend is obtained in a K_2O–Th diagram (not shown). A linear correlation is also found in a diagram of K_2O–$^{226}Ra_0$ (not shown). Therefore, once C_a^{K2O} is assumed, Th and Ra concentrations in the crustal melt can be constrained using the linear arrays in the K_2O–Th and the K_2O–$^{226}Ra_0$ diagrams. From a differentiation trend in the K_2O–SiO_2 diagram for Miyakejima rocks (Fig. 1c), we expect that the K_2O content of the crustal material does not exceed 2 wt.%. Unlike Th and Ra, K_2O is major element, and its concentration in the crustal melt is stoichiometrically controlled following melting reactions in the crust. Thus, we temporarily assume that K_2O concentration in the crustal melt does not exceed 5 wt.% (see discussion in Kuritani et al., 2005). Unknown AFC parameters, including r and ($^{230}Th/^{232}Th$)$_a$, are determined by least squares calculation of AFC trends as a function of F in K_2O–Th–($^{230}Th/^{232}Th$)–$^{226}Ra_0$ space at a given C_a^{K2O}.

Table 3 summarizes the result of the AFC calculation when C_a^{K2O} was varied from 1 to 5 wt.%. As is shown in this table, optimized C_a^{Th} and C_a^{226Ra} increase and r decreases as C_a^{K2O} increases, while optimized ($^{230}Th/^{232}Th$)$_a$ is almost constant irrespective of C_a^{K2O}. Compared to the basic model

Table 3
Optimized AFC parameters determined by the least squares method for various $C_a^{K_2O}$ values

$C_a^{K_2O}$ (wt.%)	C_a^{Th} (μg/g)	C_a^{226Ra} (fg/g)	($^{230}Th/^{232}Th$)$_a$	($^{226}Ra/^{230}Th$)$_a$	r
1.0	0.77	101	1.61	0.72	0.23
2.0	1.54	210	1.63	0.75	0.13
3.0	2.41	239	1.65	0.54	0.08
4.0	3.03	495	1.63	0.90	0.08
5.0	3.93	498	1.63	0.70	0.05

above, $(^{230}Th/^{232}Th)_a$ and r obtained are slightly high and low, respectively. The most intriguing feature is that the optimized $(^{226}Ra/^{230}Th)$ ratio in the crustal melt is not at radioactive equilibrium, but has excess ^{230}Th. This means that Th is much more incompatible to the crustal material than Ra. This is possible when the crustal material is a volcanic edifice of previous Miyakejima magmatism where plagioclase is considered to be one of the dominant mineral phases.

5.4.3. Advanced AFC model 2: ^{226}Ra decay during AFC

When the duration of AFC is not negligible compared the half-life of ^{226}Ra (1600 yr), the effect of radioactive decay during the AFC process should be taken into account. Mass-balance equations of ^{226}Ra for the AFC process can be described as follows:

$$\frac{dM_m}{dt} = \frac{dM_a}{dt} - \frac{dM_c}{dt}, \tag{2}$$

$$r = \left(\frac{dM_a}{dt}\right) \Big/ \left(\frac{dM_c}{dt}\right), \tag{3}$$

$$F = M_m/M_m^0, \tag{4}$$

$$C_m^{Ra}\frac{dM_m}{dt} + M_m\frac{dC_m^{Ra}}{dt} = C_a^{Ra}\frac{dM_a}{dt} - D^{Ra}C_m^{Ra}\frac{dM_c}{dt} - M_m\lambda^{Ra}C_m^{Ra} + M_m\lambda^{Th}C_m^{Th}\cdot\frac{A^{Ra}}{A^{Th}}, \tag{5}$$

where M_m, M_a, and M_c are mass of melt, assimilant and crystal, $M_m{}^0$ is initial mass of melt, t is time, r is the ratio of assimilation rate and crystallization rate, F is the fraction of melt remaining, C_m and C_a are concentrations in melt and assimilant, D is the bulk partition coefficient of an element between crystal and melt, λ is the decay constant, A is the atomic mass and superscripts Ra and Th represent ^{226}Ra and ^{230}Th, respectively. By substituting Eqs. (2)–(4) into (5), we obtain

$$C_m^{Ra}\frac{dF}{dt} + F\frac{dC_m^{Ra}}{dt} = \frac{r}{r-1}C_a^{Ra}\frac{dF}{dt} - \frac{1}{r-1}D^{Ra}C_m^{Ra}\frac{dF}{dt} - F\lambda^{Ra}C_m^{Ra} + F\lambda^{Th}C_m^{Th}\cdot\frac{A^{Ra}}{A^{Th}}. \tag{6}$$

For simplification, we consider that F decreases at a constant rate k, which means $F = 1 - kt$ and $dF/dt = -k$. We suppose that the assimilant maintains a constant concentration for any element throughout the AFC process. $C_m{}^{Th}$ is obtained by Eq. (1). Then, the variation of the $(^{226}Ra/^{230}Th)$ ratio in the melt can be obtained by numerical calculation of Eq. (6).

Throughout all of the Miyakejima magmatism, the highest $(^{226}Ra/^{230}Th)_0$ ratio of 3.50 is obtained in a basalt (#0115) which erupted during the 9th century (Tables 1 and 2, also see Table 1 of Yokoyama et al. (2003)). By assuming this as the starting material of AFC and applying the same AFC parameters used in Section 5.4.1, t is calculated to be 200 yr, and the F value of the most differentiated sample is 0.8. This implies that 20% by mass of the injected magma has crystallized in 200 yr before eruption. In turn, it requires >1000 yr to decrease the $(^{226}Ra/^{230}Th)$ ratio of sample #0115 from 3.50 to 2.57 (the lowest $(^{226}Ra/^{230}Th)_0$ value among all Stage 4 samples) by simple calculation of ^{226}Ra decay in a closed system. The gap is clearly due to assimilation of wall rock that has accelerated the decrease of $(^{226}Ra/^{230}Th)$ ratio in the magma injected.

Our result is strongly controlled by the composition of the injected magma. A higher $(^{226}Ra/^{230}Th)_0$ ratio than 3.50 gives t longer than 200 yr. For example, t becomes 650 yr when $(^{226}Ra/^{230}Th)_0$ ratio of the injected magma is 4.0. Furthermore, we neglected the effect of fractional crystallization that occurs while wall rock is heating up to its solidus before assimilation starts. This also results in longer t value than we obtained. In any case, however, the differentiation rate determined by the AFC model would be even faster than that for closed-system evolution in a magma chamber. Precise determination of the differentiation time with AFC might be possible by applying more advanced AFC models (e.g. Spera and Bohrson, 2001).

5.4.4. Age of assimilant

We can also apply the AFC model to ^{238}U–^{230}Th disequilibrium. The U/Th ratio of the assimilant can be determined from the AFC trend in a U–Th diagram which shows a clear linear correlation for Stage 4 samples (not shown). Importantly, the AFC trend in the U–Th diagram is not controlled by $C_a{}^{Th}$ and r value, but only by U/Th ratios of the starting material and the assimilant. From the least squares calculation, we determined that the U/Th ratio of the assimilant is 0.575, which corresponds to a $(^{238}U/^{232}Th)_a = 1.75$. As described in previous sections, $(^{230}Th/^{232}Th)_a$ is calculated to be 1.57 for the basic model and 1.61–1.65 for the advanced model 1. This gives a $(^{238}U/^{230}Th)$ ratio of the assimilant ranging from 1.06 to 1.11, implying that the assimilant is in ^{238}U–^{230}Th disequilibrium, having $(^{238}U/^{230}Th)$ greater than 1, but it is less than any of Miyakejima samples from Stage 1 to 4 (see Table 1 of Yokoyama et al. (2003)). Isshiki (1960) inferred that early Miyakejima volcanism started during the late Pleistocene. Therefore, we conclude that the assimilant would be a volcanic edifice of the Miyakejima volcano; the main cone proper that was created in the very early stages of Miyakejima volcanic activity.

6. Concluding remarks

We make the following conclusions for the geochemical evolution of Miyakejima volcano during the last 500 years. Basaltic bombs of 2000 AD had the lowest $(^{230}Th/^{232}Th)$ ratio among all of the previous Miyakejima eruptives, yielding the youngest ^{238}U–^{230}Th model age of 2 kyr. This fact reinforces our previous model that fluid release from the slab and subsequent magma generation in the mantle wedge occur episodically on a several-kyr timescale beneath Miyakejima (Yokoyama et al., 2003).

The Stage 4 samples show systematical variation in (^{230}Th/^{232}Th) and (^{226}Ra/^{230}Th) ratios against 1/Th and 1/^{230}Th, respectively. The variation cannot be explained by simple fractional crystallization with radioactive decays of ^{230}Th and ^{226}Ra. Synchronous melt generation in the mantle wedge with different upwelling speed or addition of multiple slab-derived fluids might produce the U–Th–Ra systematics of Stage 4 samples observed. However, it is much more preferable to apply assimilation and fractional crystallization (AFC) model to explain the geochemical characteristics of Stage 4 samples. In the AFC model, the U–Th–Ra systematics suggest that different batches of less differentiated magmas have been intermittently supplied from deep in the mantle, and they produced the compositional trends associated with the AFC process as observed. The assimilant is presumably a volcanic edifice of Miyakejima that was created in an earlier stage of Miyakejima magmatism.

The (^{226}Ra/^{230}Th) ratio in a magma can drastically vary when crustal assimilation is involved in magma formation, because the surrounding crust of a magma chamber generally has an age old enough to be at ^{230}Th–^{226}Ra equilibrium. This implies that the (^{226}Ra/^{230}Th) ratio in the magma is very sensitive to the effect of crustal assimilation relative to conventional isotopic tracers (Sr–Nd–Pb isotopes). Conversely, much care is needed for the estimation of magma residence time using variation of the (^{226}Ra/^{230}Th) ratio in a magma chamber (Pyle, 1992; Condomines, 1994; Condomines et al., 2003) when crustal assimilation happens during the chemical evolution of magma. U-series disequilibria in volcanic rocks, especially precise analysis of their (^{226}Ra/^{230}Th) ratio, should lead to a greater understanding of the time scale and nature of various magma processes occurring beneath an active volcano.

Acknowledgments

We thank N. Geshi for providing 2000 AD samples. We thank all the member of PML for their technical help and discussion. We are grateful to M.D. Feineman and R.J. Walker for improving the manuscript. Y. Amelin, J.B. Gill, B. Bourdon, M.R. Reid and two anonymous reviewers are thanked for their considerable efforts in reviewing the manuscript. This research was supported by Japanese Society for the Promotion of Science (JSPS) fellowships for Japanese Junior Scientists to T.Y. and T.K., Grants-in-Aid for Scientific Research from the Ministry of Education, Culture, Sports, Science and Technology, Japan (Monbu-Kagaku-sho) to E.N., and "Center of Excellence in the 21st Century in Japan" (E.N.).

Associate editor: Yuri Amelin

Appendix A. Calculation of bulk partition coefficients for Miyakejima magma

Bulk partition coefficients of U-series nuclides for the model calculations in Sections 5.2 and 5.4 are determined as follows. Yokoyama et al. (2003) examined the magma differentiation process during crystallization for all aphyric samples of Miyakejima by using the thermodynamic calculation program, MELTS (Ghiorso and Sack, 1995), and found that augite, plagioclase, magnetite and pigeonite are crystallization phases. Partition coefficients of U, Th, and Ra for these minerals can be obtained from experimental determinations, or by the lattice strain model developed by Blundy and Wood (1994). According to Blundy and Wood (2003) and references therein, D_U, D_{Th}, and D_{Ra} for these minerals are, except for D_{Ra} of plagioclase, usually quite low ($<10^{-3}$), thereby they are fixed at 10^{-3}. The partition coefficient for Ra in plagioclase is calculated from the partition coefficient of its proxy (e.g., Ba) in the lattice strain model, and D_{Ba} is a function of magma temperature and anorthite content in plagioclase. Calculated D_{Ra} ranged from 0.02 to 0.06 with plausible conditions of magma temperature and plagioclase composition determined in Kuritani et al. (2003). These estimations give bulk partition coefficients of 10^{-3} for U and Th, and 0.007-0.02 for Ra when the plagioclase proportion in the crystallizing assemblage is supposed to be 0.3. We used 0.01 for the bulk partition coefficient of Ra in the model calculations of Sections 5.2 and 5.4. For K_2O, plagioclase is the most important reservoir in the crystallization assemblage. The partition coefficient for K_2O in plagioclase is about 0.1 (e.g. McKenzie and O'Nions, 1991), and thus we used 0.03 for the bulk partition coefficient of K_2O. The variations of bulk partition coefficients of Ra and K_2O do not affect the discussions in this paper significantly.

References

Amma-Miyasaka, M., Nakagawa, M., 2002. Origin of anorthite and olivine megacrysts in island-arc tholeiites: petrological study of 1940 and 1962 ejecta from Miyake-jima volcano, Izu-Mariana arc. *J. Volcanol. Geotherm. Res.* **117**, 263–283.

Amma-Miyasaka, M., Nakagawa, M., 2003. Evolution of deeper basaltic and shallower andesitic magmas during the AD 1469–1983 eruptions of Miyake-Jima volcano, Izu-Mariana arc: inferences from temporal variations of mineral compositions in crystal-clots. *J. Petrol* **44**, 2113–2138.

Asmerom, Y., DuFrane, S.A., Mukasa, S.B., Cheng, H., Edwards, R.L., 2005. Time scale of magma differentiation in arcs from protactinium–radium isotopic data. *Geology* **33**, 633–636.

Blake, S., Rogers, N., 2005. Magma differentiation rates from (^{226}Ra/^{230}Th) and the size and power output of magma chambers. *Earth Planet. Sci. Lett.* **236**, 654–669.

Blundy, J., Wood, B., 1994. Prediction of crystal-melt partition coefficients from elastic moduli. *Nature* **372**, 452–454.

Blundy, J., Wood, B., 2003. Mineral-melt partitioning of uranium, thorium and their daughters. In: Bourdon, B., Henderson, G.M., Lundstrom, C.C., Turner, S.P. (Eds.), *Uranium-Series Geochemistry*, vol. 52. Geochemical Society, Mineralogical Society of America, pp. 59–123.

Bourdon, B., Henderson, G.M., Lundstrom, C.C., Turner, S.P., 2003. *Uranium-Series Geochemistry*. Geochemical Society, Mineralogical Society of America.

Cheng, H., Edwards, R.L., Hoff, J., Gallup, C.D., Richards, D.A., Asmerom, Y., 2000. The half-lives of uranium-234 and thorium-230. *Chem. Geol.* **169**, 17–33.

Condomines, M., 1994. Comment on: "The volume and residence time of magma beneath active volcanoes determined by decay series disequilibria methods". *Earth Planet. Sci. Lett.* **122**, 251–255.

Condomines, M., Gauthier, P.-J., Sigmarsson, O., 2003. Timescales of magma chamber processes and dating of young volcanic rocks. In: Bourdon, B., Henderson, G.M., Lundstrom, C.C., Turner, S.P. (Eds.), *Uranium-Series Geochemistry*, vol. 52. Geochemical Society, Mineralogical Society of America, pp. 125–174.

Condomines, M., Tanguy, J.-C., Michaud, V., 1995. Magma dynamics at Mt Etna: Constraints from U–Th–Ra–Pb radioactive disequilibria and Sr isotopes in historical lavas. *Earth Planet. Sci. Lett.* **132**, 25–41.

Cooper, K.M., Goldstein, S.J., Sims, K.W.W., Murrell, M.T., 2003. Uranium-series chronology of Gorda Ridge volcanism: new evidence from the 1996 eruption. *Earth Planet. Sci. Lett.* **206**, 459–475.

Cooper, K.M., Reid, M.R., Murrell, M.T., Clague, D.A., 2001. Crystal and magma residence at Kilauea Volcano, Hawaii: ^{230}Th–^{226}Ra dating of the 1955 east rift eruption. *Earth Planet. Sci. Lett.* **184**, 703–718.

DePaolo, D.J., 1981. Trace element and isotopic effects of combined wallrock assimilation and fractional crystallization. *Earth Planet. Sci. Lett.* **53**, 189–202.

Fujii, T., Aramaki, S., Fukuoka, T., Chiba, T., 1984. Petrology of the ejecta and lavas of the 1983 eruption of Miyake-jima. *Bull. Volcanol. Soc. Jpn.* **29**, S266–S282.

George, R., Turner, S., Hawkesworth, C., Morris, J., Nye, C., Ryan, J., Zheng, S.H., 2003. Melting processes and fluid and sediment transport rates along the Alaska–Aleutian arc from an integrated U–Th–Ra–Be isotope study. *J. Geophys. Res.* **108** (No.B5). doi:10.1029/2002JB001916.

Geshi, N., Shimano, T., Chiba, T., Nakada, S., 2002a. Caldera collapse during the 2000 eruption of Miyakejima Volcano, Japan. *Bull. Volcanol.* **64**, 55–68.

Geshi, N., Shimano, T., Nagai, M., Nakada, S., 2002b. Magma plumbing system of the 2000 eruption on Miyakejima volcano, Japan. *Bull. Volcanol. Soc. Jpn.* **47**, 419–434.

Ghiorso, M.S., Sack, R.O., 1995. Chemical mass transfer in magmatic processes IV. A revised and internally consistent thermodynamic model for the interpolation and extrapolation of liquid–solid equilibria in magmatic systems at elevated temperatures and pressures. *Contrib. Mineral. Petrol.* **119**, 197–212.

Goldstein, S.J., Stirling, C.H., 2003. Techniques for measuring uranium-series nuclides: 1992–2002. In: Bourdon, B., Henderson, G.M., Lundstrom, C.C., Turner, S.P. (Eds.), *Uranium-Series Geochemistry*, vol. 52. Geochemical Society, Mineralogical Society of America, pp. 23–57.

Hawkesworth, C., George, R., Turner, S., Zellmer, G., 2004. Time scales of magmatic processes. *Earth Planet. Sci. Lett.* **218**, 1–16.

Hughes, R.D., Hawkesworth, C.J., 1999. The effects of magma replenishment processes on ^{238}U–^{230}Th disequilibrium. *Geochim. Cosmochim. Acta* **63**, 4101–4110.

Imai, N., Terashima, S., Itoh, S., Ando, A., 1995. 1994 compilation values for GSJ reference samples, "Igneous rock series". *Geochem. J.* **29**, 91–95.

Isshiki, N., 1960. Explanatory text of the geological map of Japan (Scale 1:50,000): Miyakejima (in Japanese with English abstract). Geological Survey of Japan.

Ivanovich, M., Harmon, R.S., 1992. *Uranium-Series Disequilibrium: Applications to Earth, Marine, and Environmental Sciences*. Oxford University Press.

Jaffey, A.H., Flynn, K.F., Glendenin, L.E., Bentley, W.C., Essling, A.M., 1971. Precision measurements of half-lives and specific activities of ^{235}U and ^{238}U. *Phys. Rev. C* **4**, 1889.

Kuritani, T., Kitagawa, H., Nakamura, E., 2005. Assimilation and fractional crystallization controlled by transport process of crustal melt: implications from an alkali basalt-dacitic suite from Rishiri volcano, Japan. *J. Petrol* **46**, 1421–1442.

Kuritani, T., Nakamura, E., 2003. Highly precise and accurate isotopic analysis of small amounts of Pb using ^{205}Pb–^{204}Pb and ^{207}Pb–^{204}Pb, two double spikes. *J. Anal. Atom. Spectrom.* **18**, 1464–1470.

Kuritani, T., Yokoyama, T., Kobayashi, K., Nakamura, E., 2003. Shift and rotation of composition trends by magma mixing: 1983 eruption at Miyake-jima Volcano, Japan. *J. Petrol* **44**, 1895–1916.

Le Roux, L.J., Glendenin, L.E., 1963. Half-life of ^{232}Th. In: *Proc. Natl. Meet. on Nuclear Energy*, Pretorica, S. Africa, pp. 83–94.

McKenzie, D., O'Nions, R.K., 1991. Partial melt distributions from inversion of rare earth element concentrations. *J. Petrol* **32**, 1021–1091.

Nakada, S., Nagai, M., Yasuda, A., Shimano, T., Geshi, N., Ohno, M., Akimasa, T., Kaneko, T., Fujii, T., 2001. Chronology of the Miyakejima 2000 eruption: Characteristics of summit collapsed crater and eruption products (in Japanese with English abstract). *J. Geogr.* **110**, 168–180.

Nakamura, E., Makishima, A., Moriguti, T., Kobayashi, K., Sakaguchi, C., Yokoyama, T., Tanaka, R., Kuritani, T., Takei, H., 2003. Comprehensive geochemical analyses of small amounts (<100 mg) of extraterrestrial samples for the analytical competition related to the sample return mission MUSES-C. *Inst. Space Astronaut. Sci. Rep. SP.* **16**, 49–101.

Pyle, D.M., 1992. The volume and residence time of magma beneath active volcanoes determined by decay-series disequilibria methods. *Earth Planet. Sci. Lett.* **112**, 61–73.

Soya, T., Uto, K., Makimoto, H., Kamata, H., Okumura, K., Suto, S., 1984. Bulk and mineral chemistry of lavas and ejecta of the 1983 eruption of Miyakejima volcano (in Japanese with English abstract). *Bull. Volcanol. Soc. Jpn.* **29**, S283–S296.

Spera, F.J., Bohrson, W.A., 2001. Energy-constrained open-system magmatic processes I: General model and energy-constrained assimilation and fractional crystallization (EC-AFC) formulation. *J. Petrol* **42**, 999–1018.

Tsukui, M., Suzuki, Y., 1998. Eruption history of Miyakejima volcano during the last 7000 years (in Japanese with English abstract). *Bull. Volcanol. Soc. Jpn.* **43**, 149–166.

Turner, S., George, R., Jerram, D.A., Carpenter, N., Hawkesworth, C., 2003. Case studies of plagioclase growth and residence times in island arc lavas from Tonga and the Lesser Antilles, and a model to reconcile discordant age information. *Earth Planet. Sci. Lett.* **214**, 279–294.

Vigier, N., Bourdon, B., Joron, J.L., Allegre, C.J., 1999. U-decay series and trace element systematics in the 1978 eruption of Ardoukoba, Asal rift: timescale of magma crystallization. *Earth Planet. Sci. Lett.* **174**, 81–97.

Yokoyama, T., Kobayashi, K., Kuritani, T., Nakamura, E., 2003. Mantle metasomatism and rapid ascnet of slab components beneath island arc: evidence from ^{228}U–^{230}Th–^{226}Ra disequilibria of Miyakejima volcano, Izu arc, Japan. *J. Geophys. Res.* **108** (No. B7). doi:10.1029/2002JB002103.

Yokoyama, T., Makishima, A., Nakamura, E., 1999a. Evaluation of the coprecipitation of incompatible trace elements with fluoride during silicate rock dissolution by acid digestion. *Chem. Geol.* **157**, 175–187.

Yokoyama, T., Makishima, A., Nakamura, E., 1999b. Separation of thorium and uranium from silicate rock samples using two commercial extraction chromatographic resins. *Anal. Chem.* **71**, 135–141.

Yokoyama, T., Makishima, A., Nakamura, E., 2001. Precise analysis of ^{234}U/^{238}U ratio using UO_2^+ ion with thermal ionization mass spectrometry for natural samples. *Chem. Geol.* **181**, 1–12.

Yokoyama, T., Nakamura, E., 2004. Precise analysis of radium isotope ratio for short-lived U-series disequilibria in natural samples by total evaporation thermal ionization mass spectrometry (TE-TIMS). *J. Anal. Atom. Spectrom.* **19**, 717–727.